H. Wang[1], Y. P. Li[1,2], Y. R. Liu[1], G. H. Huang[1,2]

[1]Environment and Energy Systems Engineering Research Center, School of Environment, Beijing Normal University, Beijing 100875, China

[2]Institute for Energy, Environment and Sustainable Communities, University of Regina, Regina, Saskatchewan S4S0A2, Canada

Corresponding author: Y. P. Li (yongping.li@iseis.org)

Key Points:

- Among four scenarios, the uncertainty of temperature projections would be highest under radical development scenario.
- The annual scales features dominant the relationships between temperature and factors, which can be identified by SCA downscaling model.
- Ensemble downscaling can reduce the uncertainty (i.e., numerical fluctuation and the complexity of the modes) of temperature projections.

Abstract

Assessing the impacts of multiple sources on statistical downscaling is challenged by uncertainty from global climate model (GCM), scenario and factor. In our study, by integrating stepwise cluster analysis (SCA), wavelet-based multiscale entropy (WME), and multi-level factorial analysis (MFA); a SCA-WME-MFA is developed to quantitatively analyze the diverse uncertainty (i.e., numerical fluctuation, and the complexity of the modes) of daily mean temperatures (Tmean) for Amu Darya River Basin (ADRB). The major results reveal that: (i) the most remarkable warming rate would be obtained (0.056 ± 0.015 $\circ$C/year) under SSP5-8.5; (ii) Compared to the base period (1979–2005), Tmean under SSP1-2.6, SSP2-4.5, SSP3-7.0, and SSP5-8.5 would increase by 1.06 ± 1.26 $\circ$C,1.38 ± 1.39 $\circ$C, 1.741 ± 1.255 $\circ$C, and 2.05 ± 1.22 $\circ$C in the future (2022-2097); (iii) the secular mode of temperature projections is complex (WME values = 0.81 $\pm$ 0.15), while the short-term mode is relatively single (WME values = 0.14 $\pm$ 0.13); (iv), the uncertainty of temperature projections would increase under the resource and energy intensive development scenario SSP5-8.5; (v) the annual scales features of temperature projections has a marked impact on the relationships between Tmean and factors, and they can be identified by SCA model; (vi) air temperature at 850 hPa has dominant effect on the numerical fluctuation, and the interactions of geopotential height at 500 hPa on other factors have significant effects on downscaling processes; (vii) the ensemble downscaling based on multi-GCM datasets can reduce the diverse uncertainty of temperature projections.

1 Introduction

Climate change is one of the key issues due to its effects on ecosystems and human societies over the world (He et al., 2021; Shrestha and Wang, 2020). Global

climate models (GCMs) are common tools to provide multi-model climate projections for impact studies, such as those archived in Phase 6 of the Coupled Model Intercomparison Project (CMIP6) (Almazroui et al., 2020; Cook et al., 2020; Han et al., 2020; Ukkola et al., 2020). Despite the improvement and proliferation, the coarse resolution limits GCMs describe climatic characteristics precisely for regional to local scale climate impact studies, such as hydrologic modeling and water resources assessment (Fang et al., 2015; Mishra et al., 2020; Nuterman et al., 2021). Thus, the downscaling techniques are desired to get more reliable information for local climatic characteristics.

Statistical downscaling and dynamical downscaling are two commonly downscaling techniques to tackle the scale mismatch issues (Fowler et al., 2007; Lam and Fu, 2009). Statistical downscaling, based on the statistical relationships between large-scale meteorological predictors and local predictand, provides faster and computationally efficient simulations of local climate (Gebrechorkos et al., 2019; Li et al., 2020). Compared to dynamical models, statistical downscaling techniques are more appropriate when station data for impact assessment or extreme events are required and resources are limited (Fowler and Wilby, 2007). Previously. many statistical downscaling techniques have previously been developed for the multiple scenario ensemble projections to quantify uncertainty in climate change impacts (Fan et al., 2021; Hou et al., 2017; Jacobeit et al., 2014; Jafarzadeh et al., 2021; Trinh et al., 2021). For example, Jafarzadeh et al. (2021) employed support vector machine (SVM) for downscaling daily precipitation in Iran; results indicated it has acceptable prediction skill. As a robust approach for statistical downscaling, Stepwise cluster analysis (SCA) captures nonlinear interactions between atmospheric variables and local observations as a cluster tree without requiring assumption of determined functions (Duan et al., 2021; X Q Wang et al., 2013; Zhai et al., 2019). For instance, Duan et al. (2021) used SCA to investigate the possible changes in temperature and precipitation in the Pearl River Basin, the results indicated SCA showed a reasonable simulation skill in projecting the two variables.

Despite the advantages, the statistical downscaling processes usually involve multiple uncertainty, and no statistical downscaling techniques (e.g., SCA) can identify and solve them alone. Multiple GCMs yield a wide range of projection intervals due to their structural differences (Shiru et al., 2019). Meanwhile, because of the different Shared Socioeconomic Pathways (SSPs) and Representative Concentration Pathways (RCPs), scenario uncertainty occurs inevitably resulting from different combinations of socioeconomic development pathways and climate outcomes (O'Neill et al., 2016). Hence, GCMs, scenarios, and other uncertainty sources may lead to the numerical fluctuation of downscaling results; systematic assessment of uncertainty (i.e., numerical fluctuation) from various sources in the statistical downscaling is necessary to obtain more reliable projections (De Niel et al., 2019; Liao et al., 2009; Muller et al., 2021; Nury et al., 2019; Slangen and van de Wal, 2011; Timm, 2017). Timm. (2017) presented a statistical method to estimates warming rates and their uncertainty for the northern subtropical Pacific; results showed that the largest uncertainty stems from the

emission scenarios for the late 21st century. De Niel et al. (2019) used the analysis of variance to quantify contributions of different sources to uncertainty of hydrologic processes; results showed the most important uncertainty sources in hydrological extremes projections are the GCMs. In fact, Besides GCM and scenario, factor (independent variable in statistical relationship) is also the crucial roles and one major uncertainty source for statistical downscaling processes. Every factor in the combination projection has diverse effects on projection responses. Searching main factor and quantifying the interactions of factors are important to obtaining the accurate projections results. However, few study about quantitative analysis of factor uncertainty was reported. As a powerful statistical tool, Multi-level factorial analysis (MFA) features the advantages of quantitively analyzing the effects of individual factors and their interaction on model outputs (Montgomery, 2017). Various climate change impact studies based on MFA have been reported, such as carbon dioxide mitigation plan, hydrologic, and extreme weather events (Korell et al., 2020; H Wang et al., 2021a; P P Wang et al., 2021b). Therefore, MFA is chosen to investigate the effects of multiple factors on temperature projections of statistical downscaling.

Besides the numerical fluctuation, the complexity of the modes and characteristics for time series, is part of the concept of atmospheric and hydrological variable projections uncertainty (Agarwal et al., 2016). The atmospheric and hydrological variable time series encountered in geophysics are usually non-stationary, which having one or more type of characteristics (e.g., deterministic trend, seasonality) (Roushangar et al., 2018). The non-stationary characteristics can have appreciable effects on the statistical relationships between atmospheric variables. Therefore, not only the numerical fluctuation, the complexity of modes for the atmospheric variables characteristics should be assessed to get more information about downscaling results. Wavelet transform (WT), by decomposing a time series into time–frequency space, can identify both the dominant modes of variability and how those modes vary in time (Ciria and Chiogna, 2020; Roushangar et al., 2021; Suman and Maity, 2019). For the non-stationary time series, the wavelet transform is a practical tool to analyze localized characteristics of both in temporal and frequency domains (Sehgal et al., 2014; Torrence and Compo, 1998). Meanwhile, entropy theory provides information about the uncertainty at a given scale, which can be corroborated to the level of variation present at that scale, and can serve as are reliable approach to study hydrologic and meteorologic processes (Jaynes, 1957; Singh, 1997; 2011). Wavelet-based multiscale entropy (WME), the combination of entropy theory and WT method, can measure the degree of order/disorder of the signal and carries information associated with multi-frequency signal, and evaluate the uncertainty (i.e., complexity of modes) of a time series at different timescales. WME has been applied successfully in analyzing the variability and complexity of atmospheric and hydrologic variables (Agarwal et al., 2016; Guntu et al., 2020; Karmakar et al., 2019; Roushangar et al., 2018; Ziarh et al., 2021). For instance, Guntu et al. (2020) proposed a framework based on WME for daily precipitation regionalization of Indian considering both precipitation magnitude and its temporal

variability; results indicated the integrated method reveals the unique seasonal distribution of precipitation for each region. Unfortunately, few applications of WME were reported for analysing the effects of GCM and scenario on downscaling projections results. Therefore, one potential approach for Systematically studing the uncertainty and the interactive relationship of multiple factors is to integrate techniques of SCA, WME, and MFA into a general framework.

Therefore, by integrating SCA, WME, and FA within a general framework, the objective of this study is to develop a SCA-WME-MFA framework for assessing diverse uncertainty (i.e., numerical fluctuation, and the complexity of the modes) existing in climate projections and downscaling processes for Amu Darya River Basin (ADRB) in Central Asia. Specifically, the objective entails (a) investigating the temporal change of daily mean temperatures through ensemble downscaled global climate models, (b) identifying complexity of the modes of temperature projections in multiple time scales from multi-GCM and under multi-scenario, and (c) disclosing the individual effects of multi-factor and their interactions on the numerical fluctuation of temperature projections. The results are helpful to deeply comprehend the downscaling processes and get reliable atmospheric variable projections.

2 Materials and Methods

In this study, the SCA-WME-FA method is applied to daily mean temperature data observed at twelve stations in the ADRB. Continuous Wavelet Transform (CWT) is applied to each of the observed streamflow time series using the Morlet wavelet to capture the temporal multiscale variability of the streamflow in the form of wavelet coefficients. These wavelet coefficients for each scale are utilized to obtain the entropy for the respective scales. The SCA-WME-FA consisting of three parts: (i) ensemble downscaling/projection based on multiple GCM datasets and scenarios, (ii) WME values estimation; (iii)and MFA analysis experiments. The ensemble downscaling/projection is composed of a series of simulation chains, where each chain corresponding to one GCM (total twelve GCMs) under a scenario (including SSP1-2.6, SSP2-4.5, SSP3-7.0, and SSP5-8.5) is simulated through stepwise cluster analysis (SCA) for temperature projections. Based on the results of ensemble downscaling/projection, WME method is used to estimate the entropy for different time scales (2, 4, 8, 16, 32, 64, and 128 months) for measuring the complexity of mode for every simulation chain. Then MFA is conducted to disclosing the individual effects of multi-factor and their interactions on the numerical fluctuation of temperature projections.

2.1 Stepwise cluster analysis

The stepwise cluster analysis (SCA) can describe the complicated relationship (i.e., continuous and discrete) between predictors and predictand in the form of clustering trees, and deal with the complex nonlinear and discrete relationships without assuming the functional relationship (Sun et al., 2009). Based on the characteristics under the F test, the research objects can be classified and

formed into a clustering tree through series cutting or merging processes (Su et al., 2021). Such a classification tree can be adopted to specify the inherently complex relationship between local-scale predictors and large-scale predictands (Zhu et al., 2021). Compared with other methods, SCA has the most considerable advantage in dealing with the complicated relationship between multiple dependent and independent variables at the same time.

The core content for the stepwise cluster analysis (SCA) method mainly includes two aspects: cutting (i.e., splitting one set into two) and merging (i.e., joining two sets together). The dependent variables will constantly repeat these two processes (i.e., cutting and merging) to form a cluster tree until it can no longer be cut and merged, and the two processes mainly followed a given criterion (i.e., Wilk's likelihood-ratio). The ratio is defined as follows:

(1)

where E and H are the within- and between-group sums of squares and cross products matrices, respectively.

(2)

(3)

(4)

(5)

Where e and f are the two sets of dependent variables, ne and nf are the number of the two variables and are the mean values, respectively. According to Rao's F-approximation, the Wilk's likelihood-ratio (i.e.,) for the two sets of dependent variables (i.e., e and f) can be changed to an F statistic, as follows:

(6)

As described in Wilk's likelihood-ratio criterion, if the cutting point is optimal, the value of Wilk's likelihood-ratio (i.e.,) should be the minimum. In other words, the smaller the value, the larger the difference between the two sets of dependent variables (i.e., e and f). From the formulas, the Wilk's likelihood-ratio (i.e.,) is related to the F statistic. Therefore, F test can be used here to compare the means of the two sets of dependent variables. We assume that H_0: $_e = _f$ versus H_1: $_e \quad _f$ (i.e., null and alternative hypothesis), where $_e$ and $_f$ are the population means of the two sets of dependent variables (i.e., e and f). The significance level is , if $F \quad F$, it implies that H_0 is false, and the difference between the two sets of dependent variables (i.e., e and f) is statistically significant. If $F < F$, H_0 is true, would be the merging criterion, which indicates that the two sets of dependent variables (i.e., e and f) have no significant difference.

2.2 Wavelet transform

The Continuous Wavelet Transform (CWT) Wn of a discrete sequence of observations Xn is defined as the convolution of Xn with a scaled and translated

wavelet (n). (n) depends on a non-dimensional time parameter g with zero mean and localized in both frequency and time (Farge, 1992; Torrence and Compo, 1998). The Wn is defined as:

(7)

where n is the localized time index, n 'is the time variable, s is the wavelet scale, t is the sampling period, N is the number of points in the time series, and the asterisk (*) indicates the complex conjugate. Varying the wavelet scale s and translating along the localized time index n can clarify the amplitude of any features versus the scale and how this amplitude varies with time. Since the definition of multi-scale entropies is based on the distribution of the activity in the time-frequency domain, a high degree of time-frequency localization allows an accurate measure of entropy. In this study, the Morlet wavelet function is chosen as the mother wavelet function (n) because of its good time-frequency localization when compared to the other wavelets (i.e., Mexican Hat and the Daubechies wavelets).

2.3. Multiscale wavelet entropy

To gage the complexity of the time series (i.e., the average temperature time series in this study), The wavelet coefficients produced from the CWT analysis of the time series can be utilized to obtain the multiscale wavelet entropy coefficient. Based on the Shannon entropy measure (Shannon, 1948), the multiscale wavelet entropy coefficient is defined as:

(8)

where P(xi) is the probability distribution function (pdf) describing the random behavior of variable x with the length of n. Entropy is a measure of the statistical variability of the random variable x as described by the pdf. When the base of the logarithm is log2, entropy is measured in bits. Swt is a measure of information content in the signal; more information represents a lower entropy value and vice versa. At a given scale, maximum entropy is possible when the information is evenly spread across time, and minimum entropy occurs when all the information is contained in a single location Therefore, a high value of entropy represents a high degree of unpredictability and, hence, a highly complicated and disordered system.

To measure the P(xi) in Eq. (2), an entropy based on the wavelet energy distribution of a time series was proposed Cek et al. (2009). Because the value of the entropy Swt calculated is based on the wavelet results, using this approach, by Sang et al. (2011) to propose a new entropy measure, named wavelet-based multiscale entropy (WME). According to the wavelet energy, the CWT-based pdf that P(xi) is estimated:

(9)

where P(xi) represents the wavelet energy under time position i and time scale j; E(i,j) represents the total wavelet energy of the time series under timescale j

(Cek et al., 2009; Sang et al., 2011).

2.4 Multi-level factorial analysis

MFA experiment is employed to disclose the individual and interactive effects of multiple factors on projection responses. A generalized formula can be written as y = F(x1, x2, x3, …, xn) to show this relationship, where y represents the response (i.e., dependent variable: population exposure) and (x1, x2, x3, …, xn) define the factors (i.e., independent variables: multiple factors) In the MFA experiments, the effects model of different factors (SStotal) can be outlined as two parts (Montgomery, 2017):

(10)

where SSi is the variance of the individual effect of xi; SSij to SS1, 2, …, n represent the variance of interactive effects between k factors, and all interactive terms are summarized into:

(11)

The variance fractions (%) for individual/interactive effect are calculated through the following formulas:

(12)

(13)

where i and int indicate the contribution of the individual factor and their interactive effects to the total variance, respectively

(14)

In this study, seven factors are employed, there are 37 different level combinations.

3 Study area and data

The proposed SCA-WME-FA is applied to temperature projections in the Amu Darya River Basin (ADRB) in the south of Central Asia (Figure 1). ADRB is the largest sub-basin of the Aral Sea Basin with a catchment area of nearly 465,000 km2 (Jalilov et al., 2016). The ADRB experiences a continental climate, characterized by high, dry summers and cold winter. The intense human activities (i.e., the amount of water for agriculture, hydropower generation, industrial and domestic continue to increase) significantly affect the local climate change since 1960(Chen et al., 2018; Xi and Sokolik, 2016).

The temperature variable that daily mean temperature (Tmean) of twelve stations is the predictand (Table S1). The twelve stations are located in the upper (P11 and P12), middle (P03 to P10) and lower basins (P01 to P12), respectively. The Observed dataset of twelve stations for 1979–2005 were collected from the NOAA's National Climatic Data Center (NCDC, http://ncdc.noaa.gov); the

reason for choosing the twelve stations is that their datasets have few missing values and long time span. The missing data was detected and interpolated with adjacent values prior to the downscaling. The historical meteorological variables are the predictors for training downscaling models being extracted from reanalysis datasets of the National Centers for Environmental Prediction (NCEP, https://www.esrl.noaa.gov), including relative humidity, air temperature, geopotential height, and eastward wind at different pressure levels. The meteorological variables for future period are the predictors for projecting Tmean from twelve GCMs under 4 scenarios SSP1-2.6, SSP2-4.5, SSP3-7.0, SSP5-8.5 (SSP; Shared Socioeconomic Pathway) were obtained from the Coupled Model Intercomparison Project Phase 6 (CMIP6) dataset archive (https://esgf-node.llnl.gov/search/cmip6/) (Table S2). These models were chosen for the following reasons that (1) many studies using some datasets of these GCMs have been conducted to analyze climate change in Central Asia and results demonstrated acceptable performances (Guo et al., 2021; Jiang et al., 2020); (2) these GCMs datasets were produced by different models and atmospheric circulation hypothesis, which helps provide more reliable ensemble simulation. The NECP reanalysis and GCMs datasets were resampled to the same spatial resolution through interpolation before the downscaling.

4 Result and discussion

4.1. Future temperature projection

To provide compared results, same number of predictors are selected from the three GCMs and are then used to build the SCA model. The nineteen potential predictors are selected for this study (Table 1). Since dependency across predictors may impact the performance of downscaling from SCA, the predictors are screened for collinearity by sequential forward selection prior to downscaling (Vasu and Lee, 2016). For the SCA downscaling technique, every factor is brought into SCA in turn, and the factor (e.g., TMP_850) is retained which makes the Nash coefficient the highest. Factors other than TMP_850 are brought in turn, and the factor improving the model's Nash coefficient to the greatest extent is retained, and so on until the model's Nash coefficient no longer improves. According to the results of the sequential forward selection, seven meteorological variables are selected as predictors, including TMP_850, RH_1000, RH_850, UGRD_50, HGT_500, HGT_250, and VGRD.

In calibration period, the meteorological variables from the NCEP reanalysis data during 1979–1994 were used to train the statistical downscaling model SCA for twelve stations respectively. In validation period, the trained model was validated with both of NCEP reanalysis datasets and the historical GCMs datasets from 1995 to 2005. Four goodness-of-fit statistical indicators of R^2, NSE, STD, and RMSE were calculated to assess the performances of SCA. Figure 2 and Table 2 presents the

performance of the SCA downscaling model, which is calibrated and validated with NCEP reanalysis datasets. In validation period, the mean values of R^2,

NSE, STD and RMSE for twelve stations are 0.92, 0.90, 10.40, and 4.46, respectively. To gauge the generic ability of the trained SCA model, it is validated with the GCMs historical datasets in the period of 1995–2005. Figure 3 shows the validation results with GCMs datasets of the trained model. The results of the ensemble mean are better than those of each GCM for more than half of stations (e.g., P05 to P09). For the validation results of other stations, the best results are obtained from different GCMs datasets. These results indicate that no single GCM reproduction can ensure best performance for all areas in ADRB, and ensemble projection is necessary to provide accurate temperature projections.

Figure 4 presents the changes of Tmean between the observation of stations and GCM datasets in base period (1979–2005) in different months. In general, the Tmean from GCMs datasets are less than the observations with a value of 5.35 $\pm$ 4.06 ℃, and the maximum and minimum error of Tmean are 9.43 $\pm$ 4.00 ℃ in November and 3.74 $\pm$ 0.96 ℃ in June, respectively. For a certain GCM dataset, the maximum and minimum error of Tmean are obtained from NorESM2 (7.25 $\pm$ 3.17 ℃) and IITM-ESM (4.30 $\pm$ 3.48 ℃), respectively. Meanwhile, the ensemble means are compared with the observation (Figure 5). Filled area indicates the range bounded by the maximum and minimum of the GCM reproductions; the solid red line represents the ensemble mean simulations. The observations are well captured by simulations in spring (March to May), autumn (September to November) and winter (December to February). The observations are larger than the ensemble means obviously (3.49 $\pm$ 1.09 ℃) in summer (June to August).

To investigate the long-term change, the annual trends of Tmean based on the Mann-Kendall test and Sen's slope estimator testare calculated (Libiseller and Grimvall, 2002; Mann, 1945; Sen, 1968). All the trends of Tmean are increasing, and most of them are significant (p values < 0.001), except the results from several GCMs (i.e., INM-CM, CAMS-CSM, NorESM2, MPI-ESM) under SSP1-2.6 (Figure 7). The details of Mann-Kendall tests can be seen Figure S3 in supplementary material. The range of values of Sen's slopes of Tmean are 0.013 $\pm$ 0.009 $\circ$C/year under SSP1-2.6, 0.031 $\pm$ 0.021 $\circ$C/year under SSP2-4.5, 0.046 $\pm$ 0.014 $\circ$C/year under SSP3-7.0, and 0.056 $\pm$ 0.015 $\circ$C/year) under SSP5-8.5, respectively. The highest warming rate are obtained from IITM-ESM (0.036 $\pm$ 0.001 $\circ$C/year) under SSP1-2.6, CanESM5 (0.097 $\pm$ 0.009 $\circ$C/year) under SSP2-4.5, CanESM5 (0.074 $\pm$ 0.006 $\circ$C/year) under SSP3-7.0, and IPSL-CM6A (0.081 $\pm$ 0.008 $\circ$C/year) under SSP5-8.5, respectively. Meanwhile, the lowest warming rate are from NorESM2 (0.004 $\pm$ 0.001 $\circ$C/year) under SSP1-2.6, CAMS-CSM (0.007 $\pm$ 0.001 $\circ$C/year) under SSP2-4.5, MIROC6 (0.028 $\pm$ 0.004 $\circ$C/year) under SSP3-7.0, and CanESM5 (0.040 $\pm$ 0.004 $\circ$C/year) under SSP5-8.5, respectively. The results indicate that the warming trend is likely to occur in ADRB in the future, and the warming rate would increase with the development mode turning from the sustainable (SSP1-2.6) to the radical (SSP5-8.5). The details can be seen in Table 3. Figure 6 presents the annual Tmean for the base period (1979–2005) produced by GCMs and observation. The highest and lowest Tmean are obtained from MIROC6 (13.68 $\pm$ 12.34 $\circ$C)

and CanESM5 (8.54 ± 2.19 ∘C), and the value of ensemble mean is 10.58 ± 2.34 ∘C. Compared with the observed Tmean (15.53 ± 1.93 ∘C), the downscaling results of GCMs are lower, with a percentage error of 32.3% ± 7.2%, and the results of MIROC6 have the highest accuracy, being consistent with results of (Das et al., 2018).

Figure 8 shows the average annual Tmean for all GCMs reproductions under 4 scenarios. For most reproductions, the average annual Tmean would increase with the end of the range being from low to high of future forcing pathways. In general, the Tmean under SSP1-2.6, SSP2-4.5, SSP3-7.0, and SSP5-8.5 are 6.44 ± 2.29 ∘C, 16.90 ± 2.30 ∘C, 17.27 ± 2.21 ∘C, and 17.59 ± 2.16 ∘C, respectively. For a certain GCM, The Tmean from MIROC6 are the highest under all 4 scenarios; the Tmean under SSP1-2.6, SSP2-4.5, SSP3-7.0, and SSP5-8.5 are 17.61 ± 2.06 ∘C, 19.61 ± 2.05 ∘C, 19.81 ± 1.98 ∘C, and 20.15 ± 1.97 ∘C, respectively. The results of Figure 6 and Figure 8 are compared to investigate the change of Tmean in historical (1979-2005) and future periods (2022-2097). Compared to the base period, Tmean under SSP1-2.6, SSP2-4.5, SSP3-7.0, and SSP5-8.5 would increase by 1.06 ± 1.26 ∘C, 1.38 ± 1.39 ∘C, 1.741 ± 1.255 ∘C, and 2.05 ± 1.22 ∘C, respectively. The increases from MIROC6 are the highest, and those from CESM2 are the lowest.

4.2. Multiscale entropy analysis

The Tmean time series produced by GCMs under four scenarios were distributed monthly, thus the parameters for the CWT analysis were set as $t = 1$ month (sampling time between each precipitation value), $s_0 = 2$ months (smallest scale of the wavelet) because $s = 2\ t$ (s is the wavelet scale), $_j = 0.25$ (the spacing between discrete scales), and $j_1 = 7/\ _j$ (the number of scales minus one). Scales range from S_0 up to $S_0 \times 2^{(J\ _1\ \times\ D\ _J)}$, to give a total of ($J_1$+1) scales which allows for a set of seven powers of-two with $_j$ sub-octaves each. The CWT decomposed the Tmean time series into 7 scales (i.e., 2-, 4-, 8-, 16-, 32-, 64-, and 128-month bands), respectively. Then WMEs were calculated across 7 scales for each of the Tmean time series produced by GCMs from the twelve stations (Figure 9), and WMEs represent the uncertainty of the Tmean time series at different scales. To facilitate the understanding, the 7 scales are defined as the multi-month (2- or 4-month bands), sub-annual (8-month band), annual (16-month band), multi-year (32- or 64- month band) and decadal (128- month band) scales, respectively. Summarily, for each result of GCMs or Scenarios, the highest WMEs is obtained mostly at multi-year or decadal scales (0.81 ± 0.15), while the lowest one is obtained mostly at multi-month scale (0.14 ± 0.13), indicating the secular (multi-year or decadal) mode of temperature time series has higher uncertainty than that of short-term (multi-month). This result means the secular mode of temperature time series is complex and diverse, while the short-term variation pattern is relatively single. Furthermore, the highest WME at multi-month scale would be obtained under SSP5-8.5 with values of 0.19 ± 0.16. This result indicates that, under radical development scenario, the uncertainty of atmospheric variables temperature would increase by behaviors

(e.g., exploitation of abundant fossil fuel resources) of the resource and energy intensive social mode.

Figure 10 present the WMEs values under different scenarios for three sub basins of ADRB. The highest WMEs values in sub-annual scale would be both obtained under SSP3-7.0 for upper basin and middle basins, and the highest ones in annual scale would be both obtained under SSP2-4.5 for middle and lower basins. The results indicated the uncertainty of temperature projections is similar in adjacent areas. For the middle and lower basins, the WMEs values in multi-month scale would be highest under SSP5-8.5, implying the features and modes of temperature projections are more complex for plain areas under radical development scenarios. For the whole areas of ADRB, the highest WMEs values in multi-year scales would be obtained under SSP1-2.6. This result implies that, under under the green and sustainable development scenario, not only the single trend of temperature projections (e.g., continuing warming), but also diverse characteristics and modes would exist. Figure 11 present the WME values from different GCMs. Being similar to the results of Figure 10, by the increase of time scales, the WME values would increase for every GCM and scenario. This implies that more features and modes of temperature projections would be identified under bigger time scales, and the uncertainty becomes bigger. Compared with single GCM dataset, the SCA downscaling model based on ensemble mean perform best for most stations (Figure 3 and Table 3). Meanwhile, note that all WME values of the ensemble mean in annual scale are lowest for upper (0.28), middle (0.23), and lower (0.18) basins; these results may imply that the annual scales features of atmospheric variable temperature have a marked impact on the relationships between temperature projections and factors, and these features can be identified by SCA downscaling model. According to the results of Figure 9 to Figure 11, it is effective for WME to explore the impacts of GCMs and Scenarios on the projection responses.

4.3. Individual and interactive effects of the factor on the projection responses

To identify the individual and interactive effects of the factors (i.e., predictors for the statistical downscaling models) on the projection responses of the results of MIROC6, MFA experiments are conducted. Because of the MFA results under four scenarios are similar, only the MFA results under SSP1-2.6 scenario are presented. Figure 12 shows the individual effects of every factor on temperature projections. Compared with other factors, TMP_850 has the steepest slope, implying TMP_850 has the greatest magnitude of individual effect on projected Tmean. For example, projected Tmean would increase from 8.41 to 25.08 ℃ with TMP_850 rising from its low level of -3.90 ℃ to a high level of 28.04 ℃. The lines of VGRD are close to the horizontal, meaning VGRD has very weak effects on the temperature projections. For the ADRB, the slopes of TMP_850, HGT_500 and HGT_250 are positive, meaning they have positive effects. Similarly, UGRD_50 and RH_1000 have negative effects on temperature projections. These five factors have significant individual effects on temperature projections, indicating they are closely related to temperature projections and are prefer fac-

tors for constructing the statistical downscaling model based on SCA for ADRB region. Figure 13 presents the matrix of interaction plots, which quantify the effect of each factor on temperature projections under the impact of another factor. When TMP_850 is at low level (-3.90 ℃), UGRD_50 has a negative effect (-4.23 ℃); when TMP_850 is at high level (28.04 ℃), UGRD_50 has a negative effect on temperature projections (-4.75 ℃), the impact of TMP_850 on UGRD_50 is the gap of -0.52 ℃ (12%) between the effects (row 1, column 2). The impact of HGT_500 on other factors is most significant, with a mean value of 0.27 ℃ (a variation of 25%). The interactions of HGT_500 on other factors are obvious and they should be noted for the temperature projection based on statistical downscaling. The results of MFA are conducive to identify the dominant factor and interaction between factors for the statistical downscaling processes.

5 Conclusions

In this study, a SCA-WME-MFA method was developed for quantifying diverse uncertainty existing from GCM, scenario, and factor for downscaling results. The SCA-WME-MFA features the advantages of assessing the complexity of modes for climatic variables in multi-time scales, and quantifying the individual and interactive impacts of factors on the numerical fluctuation of downscaling results. The SCA-WME-MFA was applied to quantitatively analyze the mean temperatures (i.e., Tmean) for twelve meteorological stations of ADRB in Central Asia.

The main findings can be summarized as follow: (1) SCA based on multi-GCM datasets ensemble downscaling can provide accurate temperature projections (NSE = 0.90 ± 0.3 for validation) for the areas over Central Asia; (2) the warming rate for ADRB areas would increase with the development mode in scenarios turning from the sustainable (SSP1-2.6) to the radical (SSP5-8.5), and the most remarkable one is 0.056 ± 0.015 ∘C/year; (3) Compared to the base period (1979–2005), Tmean under SSP1-2.6, SSP2-4.5, SSP3-7.0, and SSP5-8.5 would increase by 1.06 ± 1.26 ∘C,1.38 ± 1.39 ∘C, 1.741 ± 1.255 ∘C, and 2.05 ± 1.22 ∘C in the future (2022-2097); (4) the highest WMEs values are obtained mostly at multi-year or decadal scales (0.81 ± 0.15), while the lowest one is obtained mostly at multi-month scale (0.14 ± 0.13), meaning the secular mode of temperature time series is complex and diverse, while the short-term mode is relatively single; (5) the highest WME at multi-month scale would be obtained under SSP5-8.5 with values of 0.19 ± 0.16. This result indicates that, under radical development scenario, the uncertainty of atmospheric variables temperature would increase by behaviors (e.g., exploitation of abundant fossil fuel resources) of the resource and energy intensive social mode; (6) the annual scales features of atmospheric variable temperature has a marked impact on the relationships between temperature projections and factors, and these features can be identified by SCA downscaling model; (7) air temperature at 850 hPa has dominant effect on the numerical fluctuation of temperature projections, and the interactions of geopotential height at 500 hPa on other factors have significant

effects on downscaling processes; (8) the ensemble downscaling based on multi-GCM datasets can reduce the uncertainty (i.e., numerical fluctuation, and the complexity of the modes) of the temperature projections.

Acknowledgments

This research was supported by the Strategic Priority Research Program of the Chinese Academy of Sciences (Grant No. XDA20060302). The authors are grateful to the editors and the anonymous reviewers for their insightful comments and suggestions.

Open Research

The Observed dataset of twelve stations for 1979–2005 are collected from the NOAA's National Climatic Data Center (http://ncdc.noaa.gov). The historical meteorological variables are extracted from reanalysis datasets of the National Centers for Environmental Prediction (https://www.esrl.noaa.gov). The meteorological variables from twelve GCMs under 4 scenarios are obtained from the Coupled Model Intercomparison Project Phase 6 (CMIP6) dataset archive

(https://esgf node.llnl.gov/search/cmip6/).

References

Agarwal, A., R. Maheswaran, V. Sehgal, R. Khosa, B. Sivakumar, and C. Bernhofer (2016), Hydrologic regionalization using wavelet-based multiscale entropy method, *Journal of Hydrology*, *538*, 22-32, doi:10.1016/j.jhydrol.2016.03.023.Almazroui, M., F. Saeed, S. Saeed, M. N. Islam, M. Ismail, N. A. B. Klutse, and M. H. Siddiqui (2020), Projected Change in Temperature and Precipitation Over Africa from CMIP6, *Earth Syst. Environ.*, *4*(3), 455-475, doi:10.1007/s41748-020-00161-x.Chen, Y. N., Z. Li, G. H. Fang, and W. H. Li (2018), Large Hydrological Processes Changes in the Transboundary Rivers of Central Asia, *Journal of Geophysical Research-Atmospheres*, *123*(10), 5059-5069, doi:10.1029/2017jd028184.Ciria, T. P., and G. Chiogna (2020), Intra-catchment comparison and classification of long-term streamflow variability in the Alps using wavelet analysis, *Journal of Hydrology*, *587*, 20, doi:10.1016/j.jhydrol.2020.124927.Cook, B. I., J. S. Mankin, K. Marvel, A. P. Williams, J. E. Smerdon, and K. J. Anchukaitis (2020), Twenty-First Century Drought Projections in the CMIP6 Forcing Scenarios, *Earth Future*, *8*(6), 20, doi:10.1029/2019ef001461.Das, L., M. Dutta, A. Mezghani, and R. E. Benestad (2018), Use of observed temperature statistics in ranking CMIP5 model performance over the Western Himalayan Region of India, *International Journal of Climatology*, *38*(2), 554-570, doi:10.1002/joc.5193.De Niel, J., E. Van Uytven, and P. Willems (2019), Uncertainty Analysis of Climate Change Impact on River Flow Extremes Based on a Large Multi-Model Ensemble, *Water Resources Management*, *33*(12), 4319-4333, doi:10.1007/s11269-019-02370-0.Duan, R. X., G. H. Huang, Y. P. Li, X. Zhou, J. Y. Ren, and C. Y. Tian (2021), Stepwise clustering future meteorological drought projection and multi-level factorial analysis under climate change: A case study of the Pearl River Basin,

China, *Environmental Research*, *196*, 15, doi:10.1016/j.envres.2020.110368.Fan, X. W., L. Jiang, and J. J. Gou (2021), Statistical downscaling and projection of future temperatures across the Loess Plateau, China, *Weather Clim. Extremes*, *32*, 12, doi:10.1016/j.wace.2021.100328.Fang, G. H., J. Yang, Y. N. Chen, and C. Zammit (2015), Comparing bias correction methods in downscaling meteorological variables for a hydrologic impact study in an arid area in China, *Hydrology and Earth System Sciences*, *19*(6), 2547-2559, doi:10.5194/hess-19-2547-2015.Fowler, H. J., S. Blenkinsop, and C. Tebaldi (2007), Linking climate change modelling to impacts studies: recent advances in downscaling techniques for hydrological modelling, *International Journal of Climatology*, *27*(12), 1547-1578, doi:10.1002/joc.1556.Fowler, H. J., and R. L. Wilby (2007), Beyond the downscaling comparison study, *International Journal of Climatology*, *27*(12), 1543-1545, doi:10.1002/joc.1616.Gebrechorkos, S. H., S. Hulsmann, and C. Bernhofer (2019), Regional climate projections for impact assessment studies in East Africa, *Environ. Res. Lett.*, *14*(4), 14, doi:10.1088/1748-9326/ab055a.Guntu, R. K., R. Maheswaran, A. Agarwal, and V. P. Singh (2020), Accounting for temporal variability for improved precipitation regionalization based on self-organizing map coupled with information theory, *Journal of Hydrology*, *590*, 20, doi:10.1016/j.jhydrol.2020.125236.Guo, H., A. M. Bao, T. Chen, G. X. Zheng, Y. Q. Wang, L. L. Jiang, and P. De Maeyer (2021), Assessment of CMIP6 in simulating precipitation over arid Central Asia, *Atmospheric Research*, *252*, 15, doi:10.1016/j.atmosres.2021.105451.Han, J. Y., C. Y. Miao, Q. Y. Duan, J. W. Wu, X. H. Lei, and W. H. Liao (2020), Variations in start date, end date, frequency and intensity of yearly temperature extremes across China during the period 1961-2017, *Environ. Res. Lett.*, *15*(4), 12, doi:10.1088/1748-9326/ab7390.He, H. L., R. Hamdi, P. Cai, G. P. Luo, F. U. Ochege, M. Zhang, P. Termonia, P. De Maeyer, and C. F. Li (2021), Impacts of Historical Land Use/Cover Change (1980-2015) on Summer Climate in the Aral Sea Region, *Journal of Geophysical Research-Atmospheres*, *126*(6), 21, doi:10.1029/2020jd032638.Hou, Y. K., H. Chen, C. Y. Xu, J. Chen, and S. L. Guo (2017), Coupling a Markov Chain and Support Vector Machine for At-Site Downscaling of Daily Precipitation, *J. Hydrometeorol.*, *18*(9), 2385-2406, doi:10.1175/jhm-d-16-0130.1.Jacobeit, J., E. Hertig, S. Seubert, and K. Lutz (2014), Statistical downscaling for climate change projections in the Mediterranean region: methods and results, *Regional Environmental Change*, *14*(5), 1891-1906, doi:10.1007/s10113-014-0605-0.Jafarzadeh, A., M. Pourreza-Bilondi, A. K. Siuki, and J. R. Moghadam (2021), Examination of Various Feature Selection Approaches for Daily Precipitation Downscaling in Different Climates, *Water Resources Management*, *35*(2), 407-427, doi:10.1007/s11269-020-02701-6.Jaynes, E. T. (1957), INFORMATION THEORY AND STATISTICAL MECHANICS, *Phys. Rev.*, *106*(4), 620-630, doi:10.1103/PhysRev.106.620.Jiang, J., T. J. Zhou, X. L. Chen, and L. X. Zhang (2020), Future changes in precipitation over Central Asia based on CMIP6 projections, *Environ. Res. Lett.*, *15*(5), 8, doi:10.1088/1748-9326/ab7d03.Karmakar, S., S. Goswami, and S. Chattopadhyay (2019), Exploring the pre- and summer-monsoon surface air temperature over eastern India using Shannon entropy and temporal Hurst

exponents through rescaled range analysis, *Atmospheric Research*, *217*, 57-62, doi:10.1016/j.atmosres.2018.10.007.Korell, L., T. M. Sandner, D. Matthies, and K. Ludewig (2020), Effects of drought and N level on the interactions of the root hemiparasiteRhinanthus alectorolophuswith a combination of three host species, *Plant Biology*, *22*, 84-92, doi:10.1111/plb.12977.Lam, Y. F., and J. S. Fu (2009), A novel downscaling technique for the linkage of global and regional air quality modeling, *Atmos. Chem. Phys.*, *9*(23), 9169-9185, doi:10.5194/acp-9-9169-2009.Li, L., L. Lei, M. S. Zheng, A. G. L. Borthwick, and J. R. Ni (2020), Stochastic Evolutionary-Based Optimization for Rapid Diagnosis and Energy-Saving in Pilot- and Full-Scale Carrousel Oxidation Ditches, *Journal of Environmental Informatics*, *35*(1), 81-93, doi:10.3808/jei.201700377.Liao, K. J., E. Tagaris, K. Manomaiphiboon, C. Wang, J. H. Woo, P. Amar, S. He, and A. G. Russell (2009), Quantification of the impact of climate uncertainty on regional air quality, *Atmos. Chem. Phys.*, *9*(3), 865-878, doi:10.5194/acp-9-865-2009.Libiseller, C., and A. Grimvall (2002), Performance of partial Mann-Kendall tests for trend detection in the presence of covariates, *Environmetrics*, *13*(1), 71-84, doi:10.1002/env.507.Mann, H. B. (1945), Nonparametric Tests Against Trend, *Econometrica*, *13*(3), 245-259, doi:10.2307/1907187.Mishra, V., U. Bhatia, and A. D. Tiwari (2020), Bias-corrected climate projections for South Asia from Coupled Model Intercomparison Project-6, *Sci. Data*, *7*(1), 13, doi:10.1038/s41597-020-00681-1.Montgomery, D. C. (2017), *Design and analysis of experiments*, John wiley & sons.Muller, C., et al. (2021), Exploring uncertainties in global crop yield projections in a large ensemble of crop models and CMIP5 and CMIP6 climate scenarios, *Environ. Res. Lett.*, *16*(3), 16, doi:10.1088/1748-9326/abd8fc.Nury, A. H., A. Sharma, L. Marshall, and R. Mehrotra (2019), Characterising uncertainty in precipitation downscaling using a Bayesian approach, *Adv. Water Resour.*, *129*, 189-197, doi:10.1016/j.advwatres.2019.05.018.Nuterman, R., A. Mahura, A. Baklanov, B. Amstrup, and A. Zakey (2021), Downscaling system for modeling of atmospheric composition on regional, urban and street scales, *Atmos. Chem. Phys.*, *21*(14), 11099-11112, doi:10.5194/acp-21-11099-2021.O'Neill, B. C., et al. (2016), The Scenario Model Intercomparison Project (ScenarioMIP) for CMIP6, *Geosci. Model Dev.*, *9*(9), 3461-3482, doi:10.5194/gmd-9-3461-2016.Roushangar, K., F. Alizadeh, and J. Adamowski (2018), Exploring the effects of climatic variables on monthly precipitation variation using a continuous wavelet-based multiscale entropy approach, *Environmental Research*, *165*, 176-192, doi:10.1016/j.envres.2018.04.017.Roushangar, K., M. Moghaddas, R. Ghasempour, and F. Alizadeh (2021), Evaluation of spatial-temporal characteristics of precipitation using discrete maximal overlap wavelet transform and spatial clustering tools, *Hydrol. Res.*, *52*(2), 414-430, doi:10.2166/nh.2021.141.Sehgal, V., M. K. Tiwari, and C. Chatterjee (2014), Wavelet Bootstrap Multiple Linear Regression Based Hybrid Modeling for Daily River Discharge Forecasting, *Water Resources Management*, *28*(10), 2793-2811, doi:10.1007/s11269-014-0638-7.Sen, P. K. (1968), Estimates of the Regression Coefficient Based on Kendall's Tau, *Journal of the American Statistical Association*, *63*(324), 1379-1389, doi:10.1080/01621459.1968.10480934.Shiru,

M. S., S. Shahid, E. S. Chung, N. Alias, and L. Scherer (2019), A MCDM-based framework for selection of general circulation models and projection of spatio-temporal rainfall changes: A case study of Nigeria, *Atmospheric Research*, *225*, 1-16, doi:10.1016/j.atmosres.2019.03.033.Shrestha, N. K., and J. Wang (2020), Water Quality Management of a Cold Climate Region Watershed in Changing Climate, *Journal of Environmental Informatics*, *35*(1), 56-80, doi:10.3808/jei.201900407.Singh, V. P. (1997), The use of entropy in hydrology and water resources, *Hydrological Processes*, *11*(6), 587-626.Singh, V. P. (2011), Hydrologic Synthesis Using Entropy Theory: Review, *J. Hydrol. Eng.*, *16*(5), 421-433, doi:10.1061/(asce)he.1943-5584.0000332.Slangen, A. B. A., and R. S. W. van de Wal (2011), An assessment of uncertainties in using volume-area modelling for computing the twenty-first century glacier contribution to sea-level change, *Cryosphere*, *5*(3), 673-686, doi:10.5194/tc-5-673-2011.Suman, M., and R. Maity (2019), Hybrid Wavelet-ARX approach for modeling association between rainfall and meteorological forcings at river basin scale, *Journal of Hydrology*, *577*, 14, doi:10.1016/j.jhydrol.2019.123918.Timm, O. E. (2017), Future warming rates over the Hawaiian Islands based on elevation-dependent scaling factors, *International Journal of Climatology*, *37*, 1093-1104, doi:10.1002/joc.5065.Torrence, C., and G. P. Compo (1998), A practical guide to wavelet analysis, *Bull. Amer. Meteorol. Soc.*, *79*(1), 61-78, doi:10.1175/1520-0477(1998)079<0061:Apgtwa>2.0.Co;2.Trinh, T., N. Do, V. T. Nguyen, and K. Carr (2021), Modeling high-resolution precipitation by coupling a regional climate model with a machine learning model: an application to Sai Gon-Dong Nai Rivers Basin in Vietnam, *Clim. Dyn.*, 23, doi:10.1007/s00382-021-05833-6.Ukkola, A. M., M. G. De Kauwe, M. L. Roderick, G. Abramowitz, and A. J. Pitman (2020), Robust Future Changes in Meteorological Drought inCMIP6Projections Despite Uncertainty in Precipitation, *Geophys. Res. Lett.*, *47*(11), 9, doi:10.1029/2020gl087820.Vasu, N. N., and S. R. Lee (2016), A hybrid feature selection algorithm integrating an extreme learning machine for landslide susceptibility modeling of Mt. Woomyeon, South Korea, *Geomorphology*, *263*, 50-70, doi:10.1016/j.geomorph.2016.03.023.Wang, H., Y. P. Li, Y. R. Liu, G. H. Huang, Y. F. Li, and Q. M. Jia (2021a), Analyzing streamflow variation in the data-sparse mountainous regions: An integrated CCA-RF-FA framework, *Journal of Hydrology*, *596*, 14, doi:10.1016/j.jhydrol.2021.126056.Wang, P. P., Y. P. Li, G. H. Huang, S. G. Wang, C. Suo, and Y. Ma (2021b), A multi-scenario factorial analysis and multi-regional input-output model for analyzing CO2 emission reduction path in Jing-Jin-Ji region, *J. Clean Prod.*, *300*, 15, doi:10.1016/j.jclepro.2021.126782.Wang, X. Q., G. H. Huang, Q. G. Lin, X. H. Nie, G. H. Cheng, Y. R. Fan, Z. Li, Y. Yao, and M. Q. Suo (2013), A stepwise cluster analysis approach for downscaled climate projection - A Canadian case study, *Environ. Modell. Softw.*, *49*, 141-151, doi:10.1016/j.envsoft.2013.08.006.Xi, X., and I. N. Sokolik (2016), Quantifying the anthropogenic dust emission from agricultural land use and desiccation of the Aral Sea in Central Asia, *Journal of Geophysical Research-Atmospheres*, *121*(20), 12270-12281, doi:10.1002/2016jd025556.Zhai, Y. Y., G. Huang, X. Q. Wang, X. Zhou, C. Lu, and Z. Li (2019), Future projections of temperature

changes in Ottawa, Canada through stepwise clustered downscaling of multiple GCMs under RCPs, *Clim. Dyn.*, *52*(5-6), 3455-3470, doi:10.1007/s00382-018-4340-y.Ziarh, G. F., M. Asaduzzaman, A. Dewan, M. S. Nashwan, and S. Shahid (2021), Integration of catastrophe and entropy theories for flood risk mapping in peninsular Malaysia, *J. Flood Risk Manag.*, *14*(1), 13, doi:10.1111/jfr3.12686.

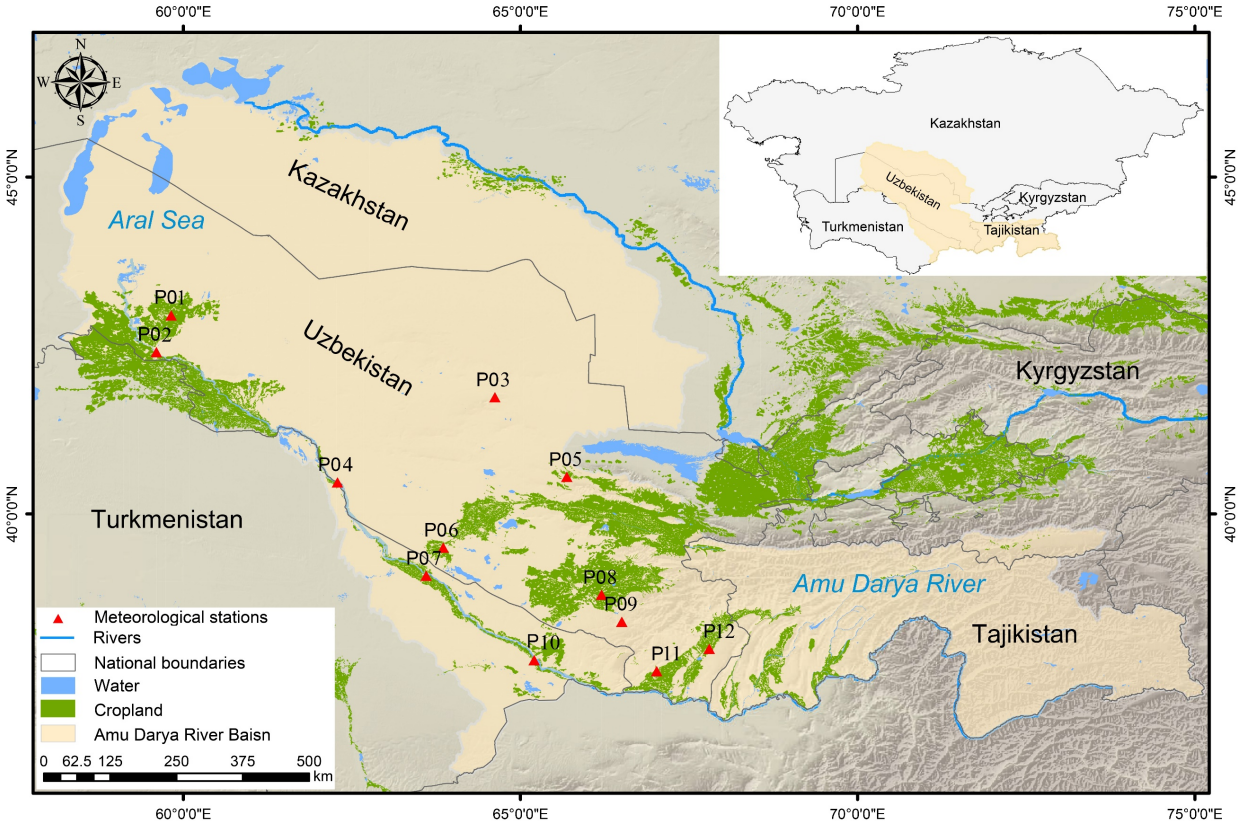

Figure 1. The map of Amu Darya River Basin and the meteorological stations.

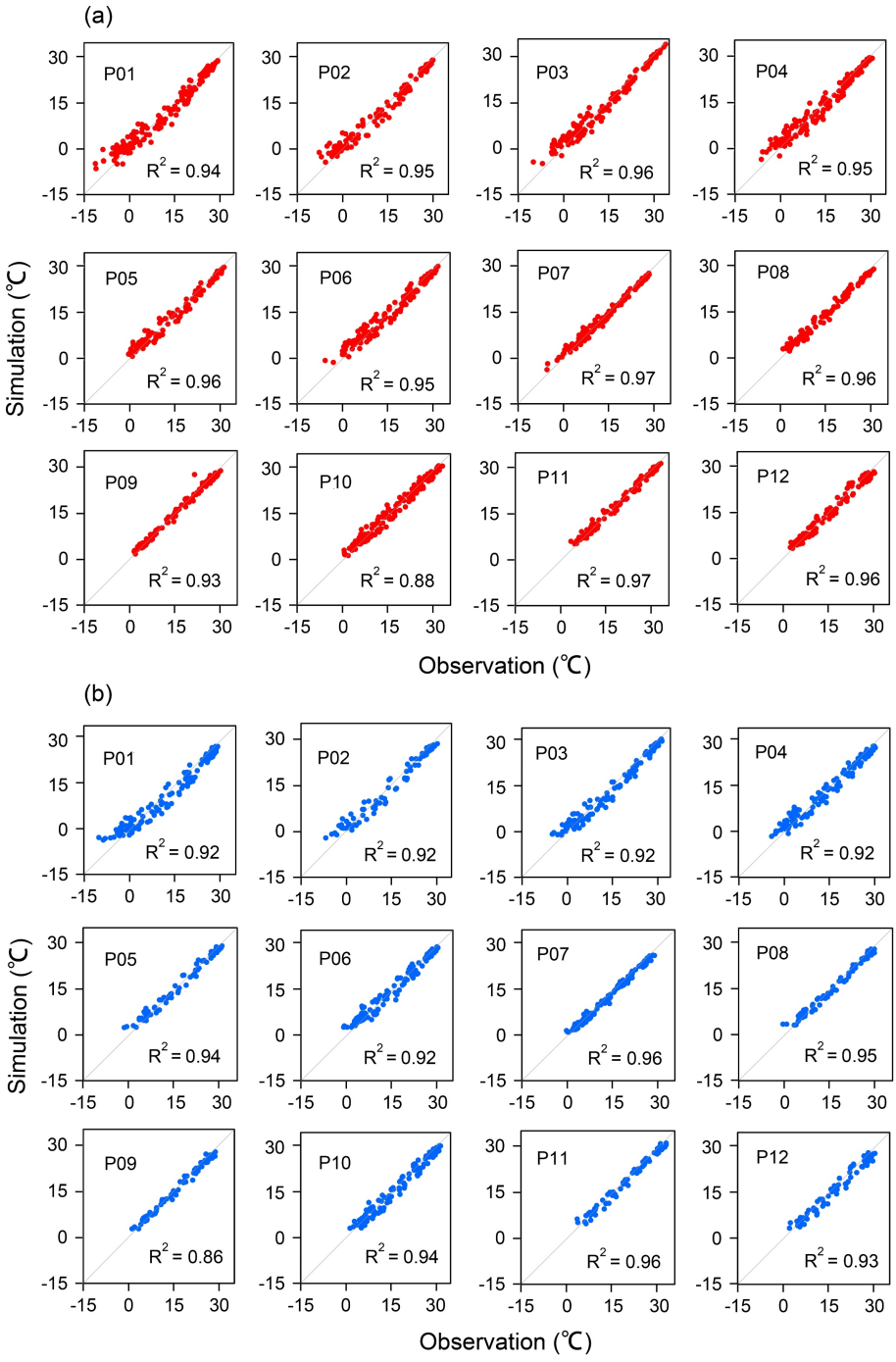

Figure 2. Calibration and validation results of GCMs' reproductions for Tmean

with NCEP reanalysis datasets.

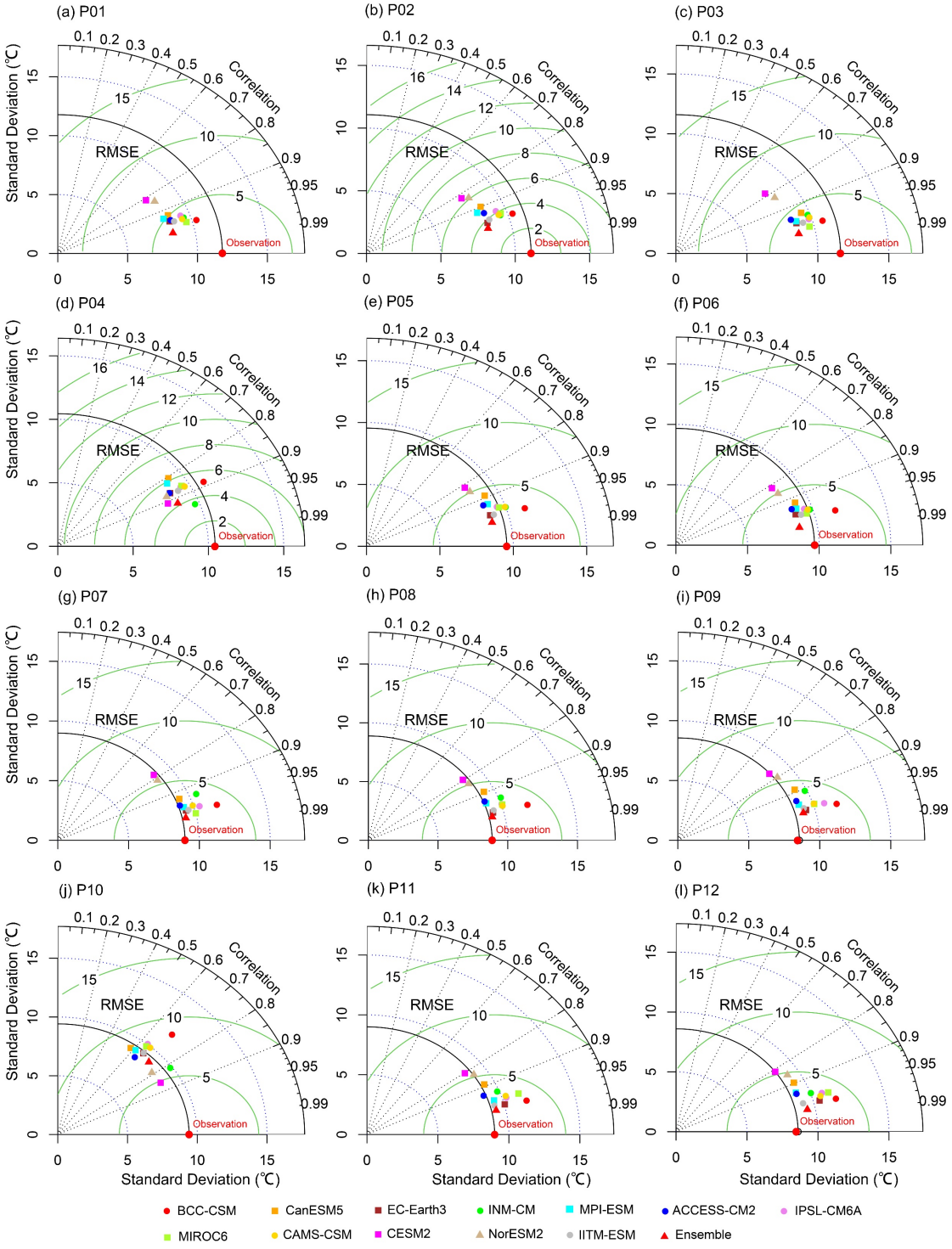
(a) P01
(b) P02
(c) P03
(d) P04
(e) P05
(f) P06
(g) P07
(h) P08
(i) P09
(j) P10
(k) P11
(l) P12
Standard Deviation (℃)
Correlation
RMSE
Observation
BCC-CSM
CanESM5
EC-Earth3
INM-CM
MPI-ESM
ACCESS-CM2
IPSL-CM6A
MIROC6
CAMS-CSM
CESM2
NorESM2
IITM-ESM
Ensemble

Figure 3. Calibration and validation results of GCMs reproductions for Tmean with historical GCMs datasets.

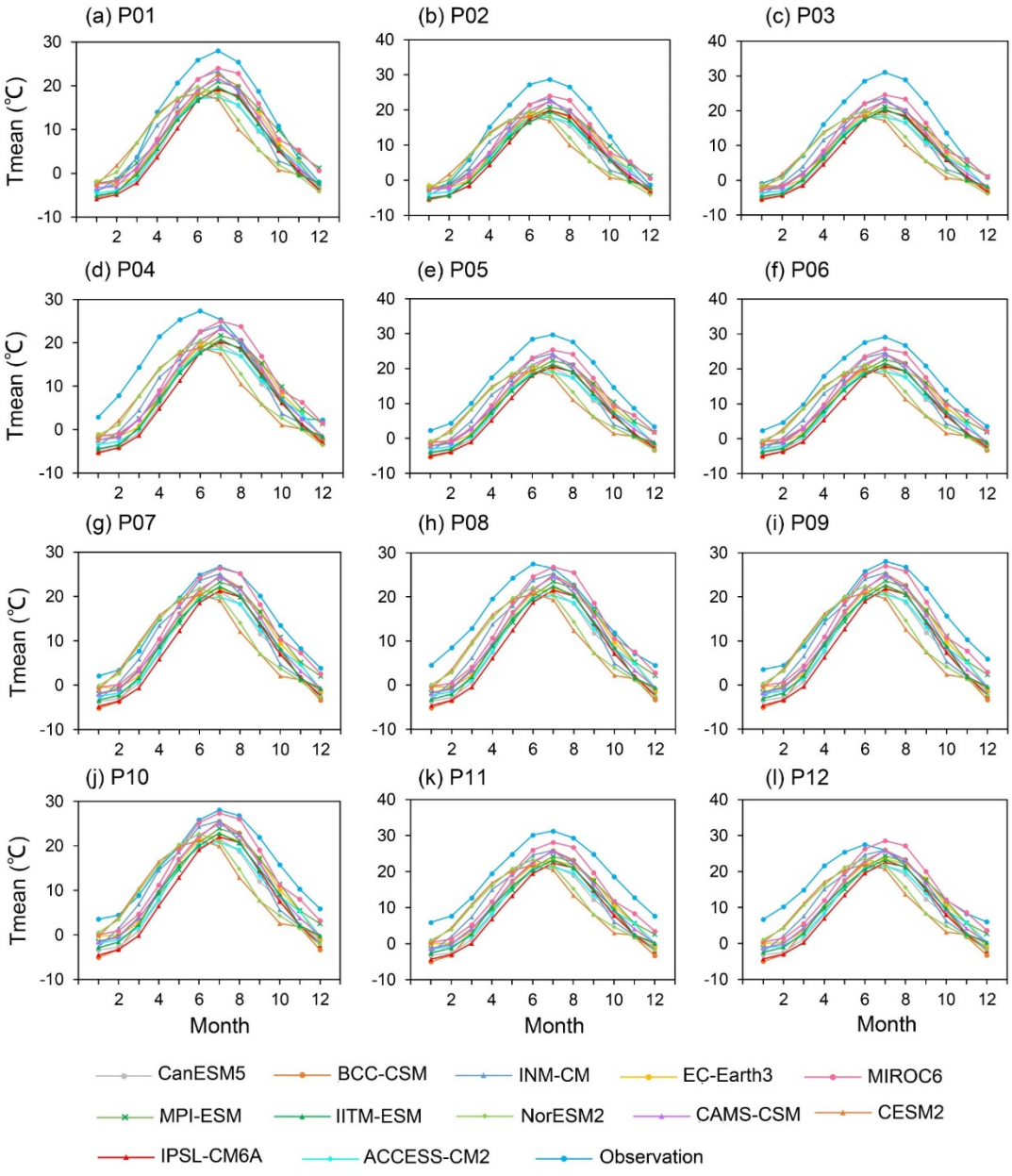

Figure 4. Monthly mean Tmean for the observed and reproductions from GCMs, 1979–2005.

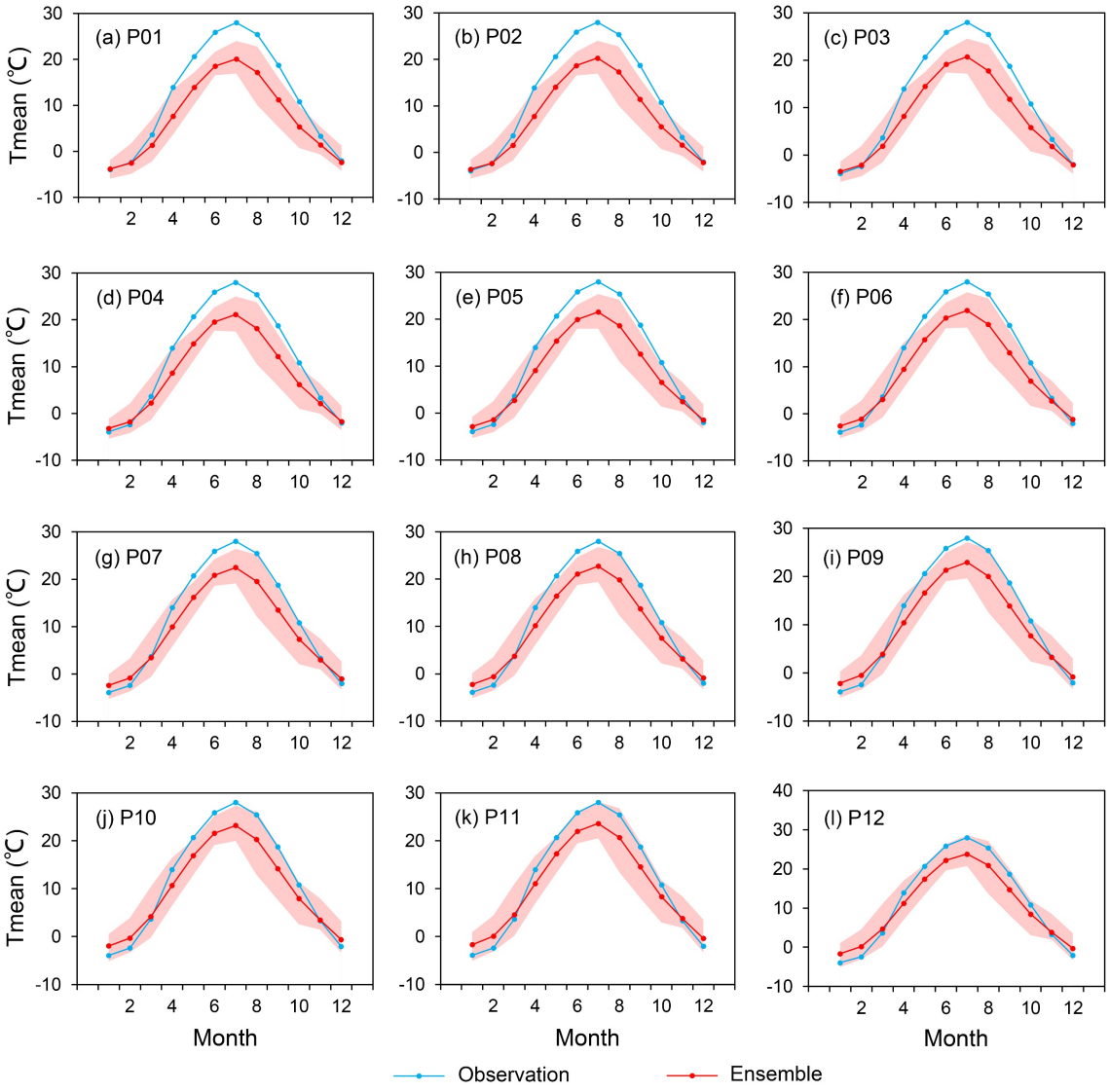

Figure 5. Monthly mean Tmean for the observed and ensemble mean of reproductions, 1979–2005.

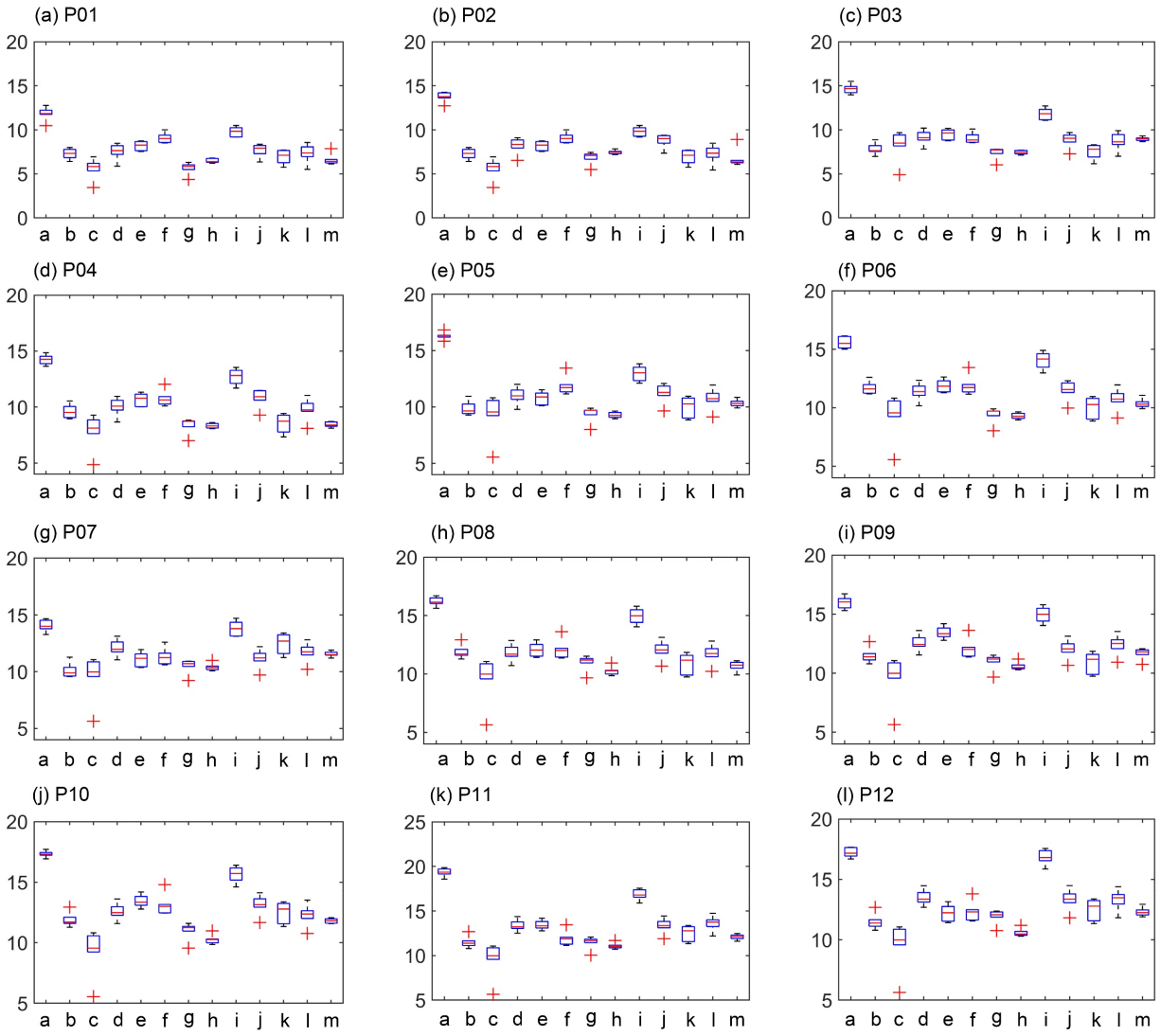

Figure 6. Comparisons of annual Tmean between GCMs' reproductions, ensemble means, and the observations for 1979–2005.

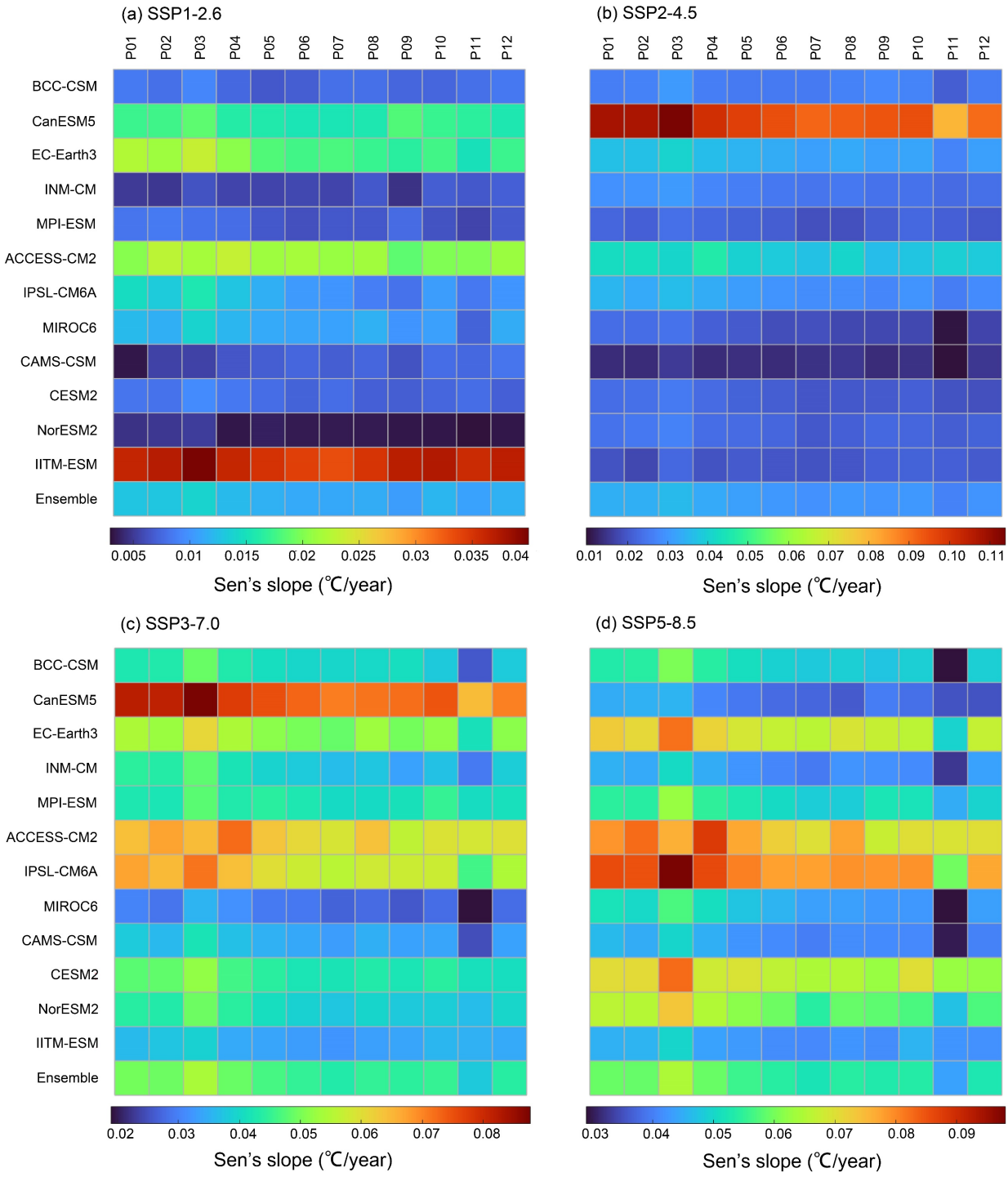
(a) SSP1-2.6
P01
P02
P03
P04
P05
P06
P07
P08
P09
P10
P11
P12
BCC-CSM
CanESM5
EC-Earth3
INM-CM
MPI-ESM
ACCESS-CM2
IPSL-CM6A
MIROC6
CAMS-CSM
CESM2
NorESM2
IITM-ESM
Ensemble
0.005
0.01
0.015
0.02
0.025
0.03
0.035
0.04
Sen's slope (℃/year)
(b) SSP2-4.5
P01
P02
P03
P04
P05
P06
P07
P08
P09
P10
P11
P12
0.01
0.02
0.03
0.04
0.05
0.06
0.07
0.08
0.09
0.10
0.11
Sen's slope (℃/year)
(c) SSP3-7.0
BCC-CSM
CanESM5
EC-Earth3
INM-CM
MPI-ESM
ACCESS-CM2
IPSL-CM6A
MIROC6
CAMS-CSM
CESM2
NorESM2
IITM-ESM
Ensemble
0.02
0.03
0.04
0.05
0.06
0.07
0.08
Sen's slope (℃/year)
(d) SSP5-8.5
0.03
0.04
0.05
0.06
0.07
0.08
0.09
Sen's slope (℃/year)

Figure 7. Annual trend of Tmean for 12 stations under 4 scenarios (2021−2100).

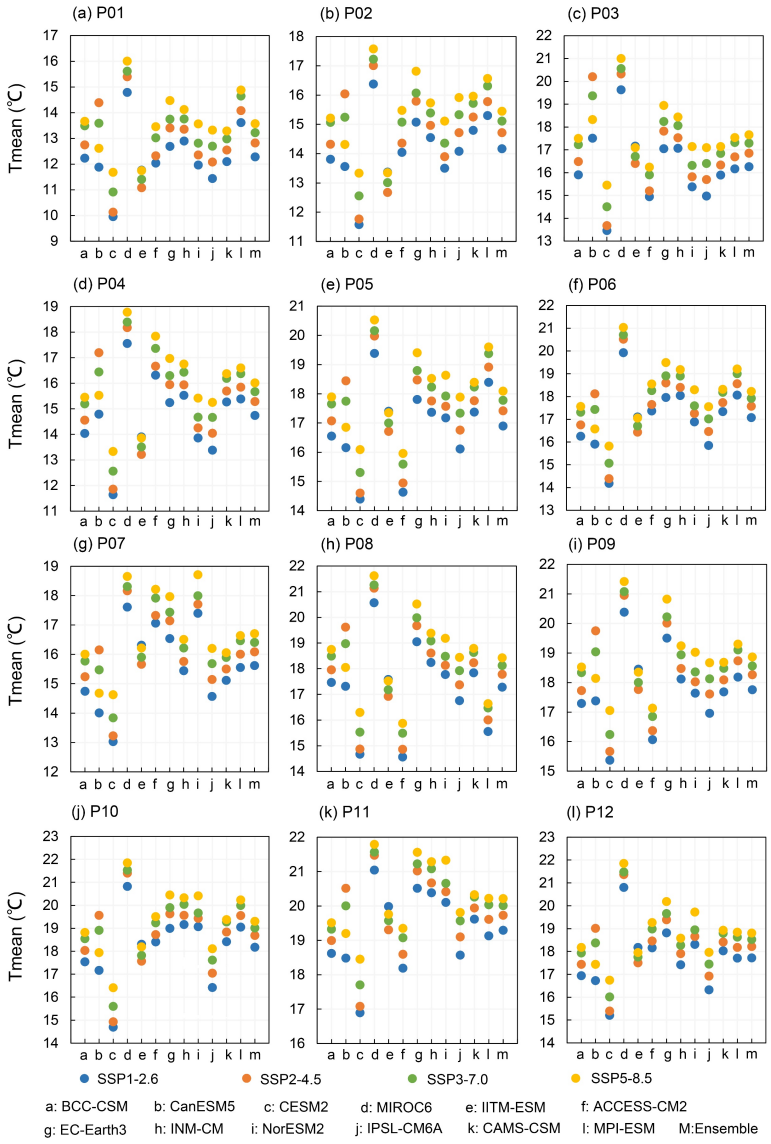

Figure 8. Comparison of annual average Tmean under 4 scenarios.

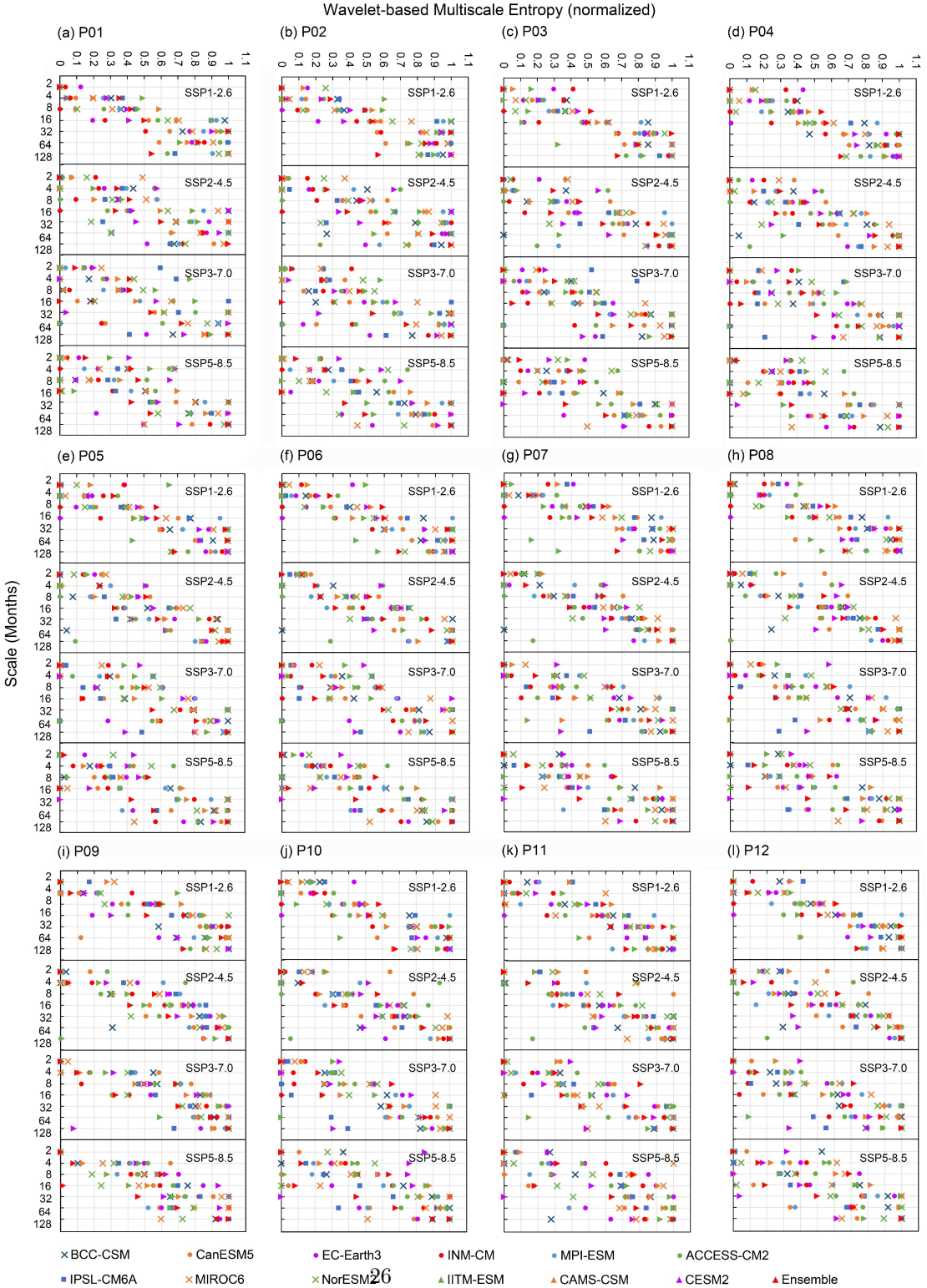
Wavelet-based Multiscale Entropy (normalized)
Scale (Months)
(a) P01
(b) P02
(c) P03
(d) P04
(e) P05
(f) P06
(g) P07
(h) P08
(i) P09
(j) P10
(k) P11
(l) P12
SSP1-2.6
SSP2-4.5
SSP3-7.0
SSP5-8.5
BCC-CSM
CanESM5
EC-Earth3
INM-CM
MPI-ESM
ACCESS-CM2
IPSL-CM6A
MIROC6
NorESM2
IITM-ESM
CAMS-CSM
CESM2
Ensemble

Figure 9. Comparison of Wavelet-based Multiscale Entropy (WME) for each scale for Tmean under 4 scenarios.

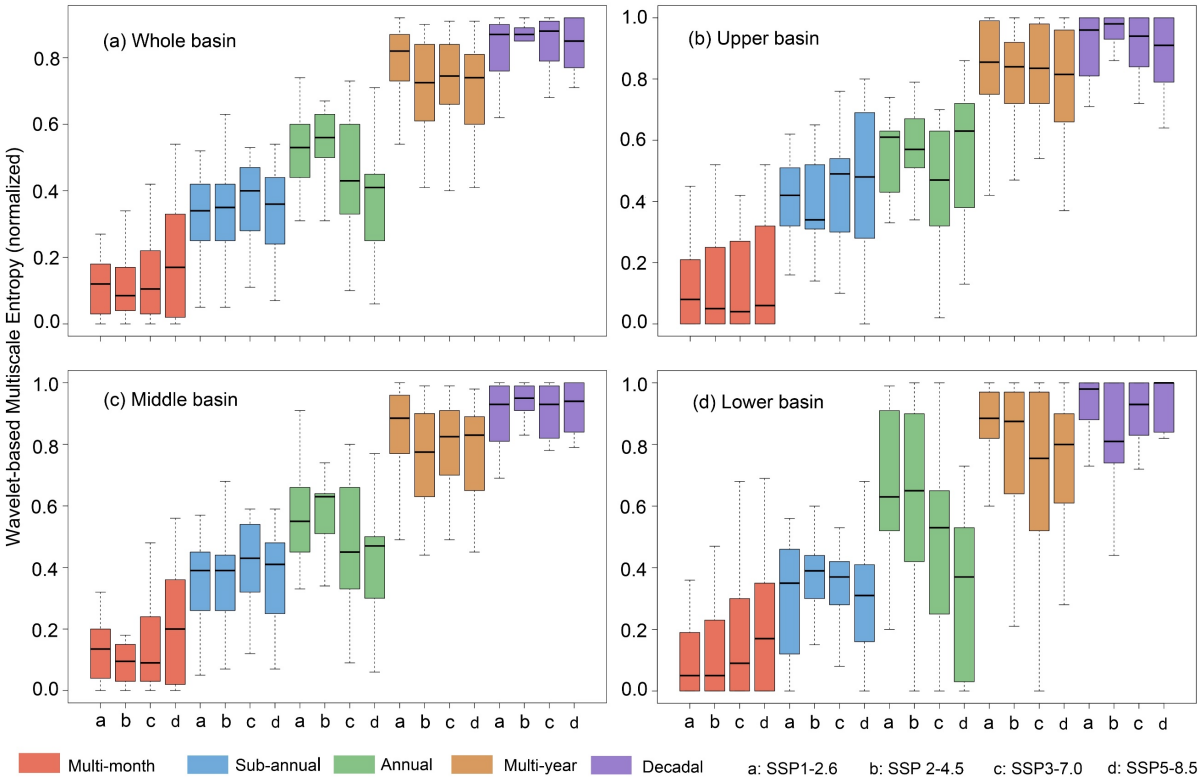

Figure 10. The effects of scenarios on the WME.

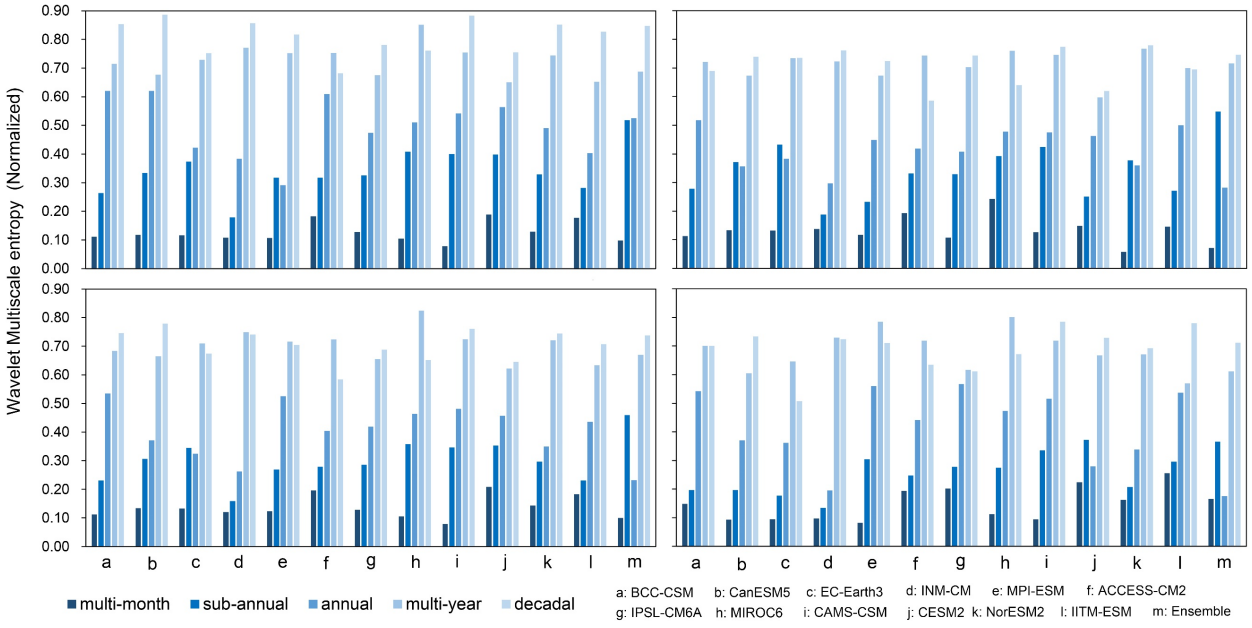

Figure 11. The effects GCMs on the WME.

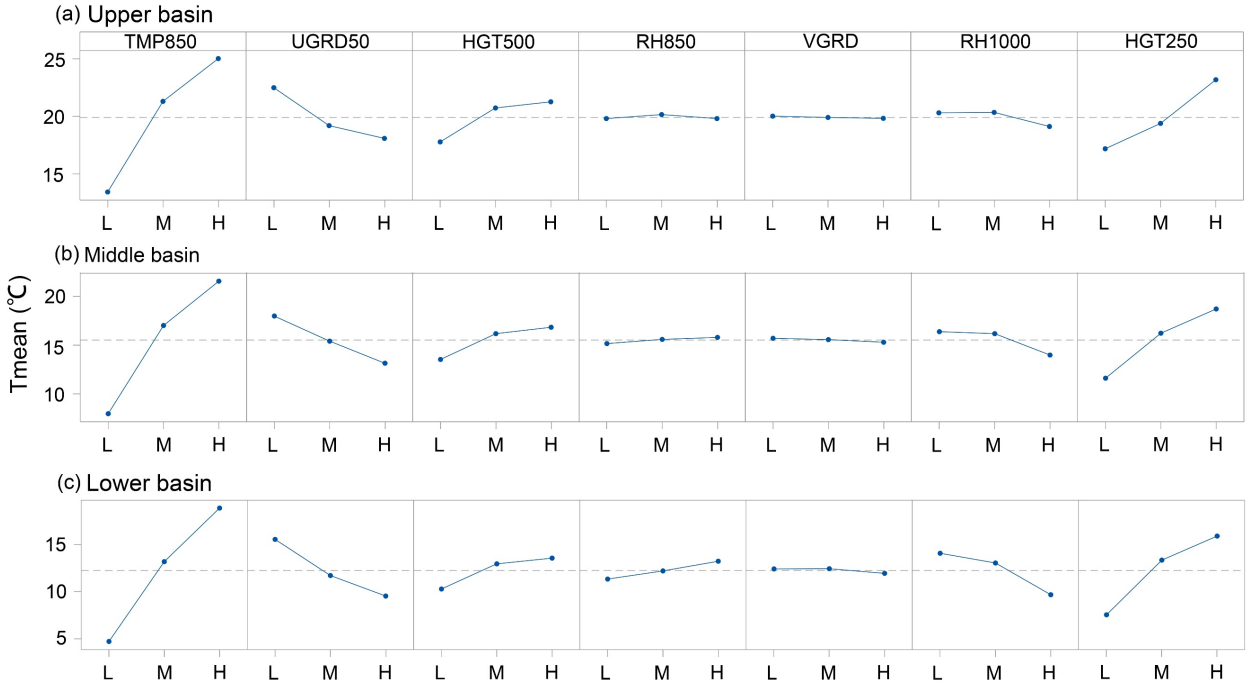

Figure 12. The main effects of factors on the Tmean projectios.

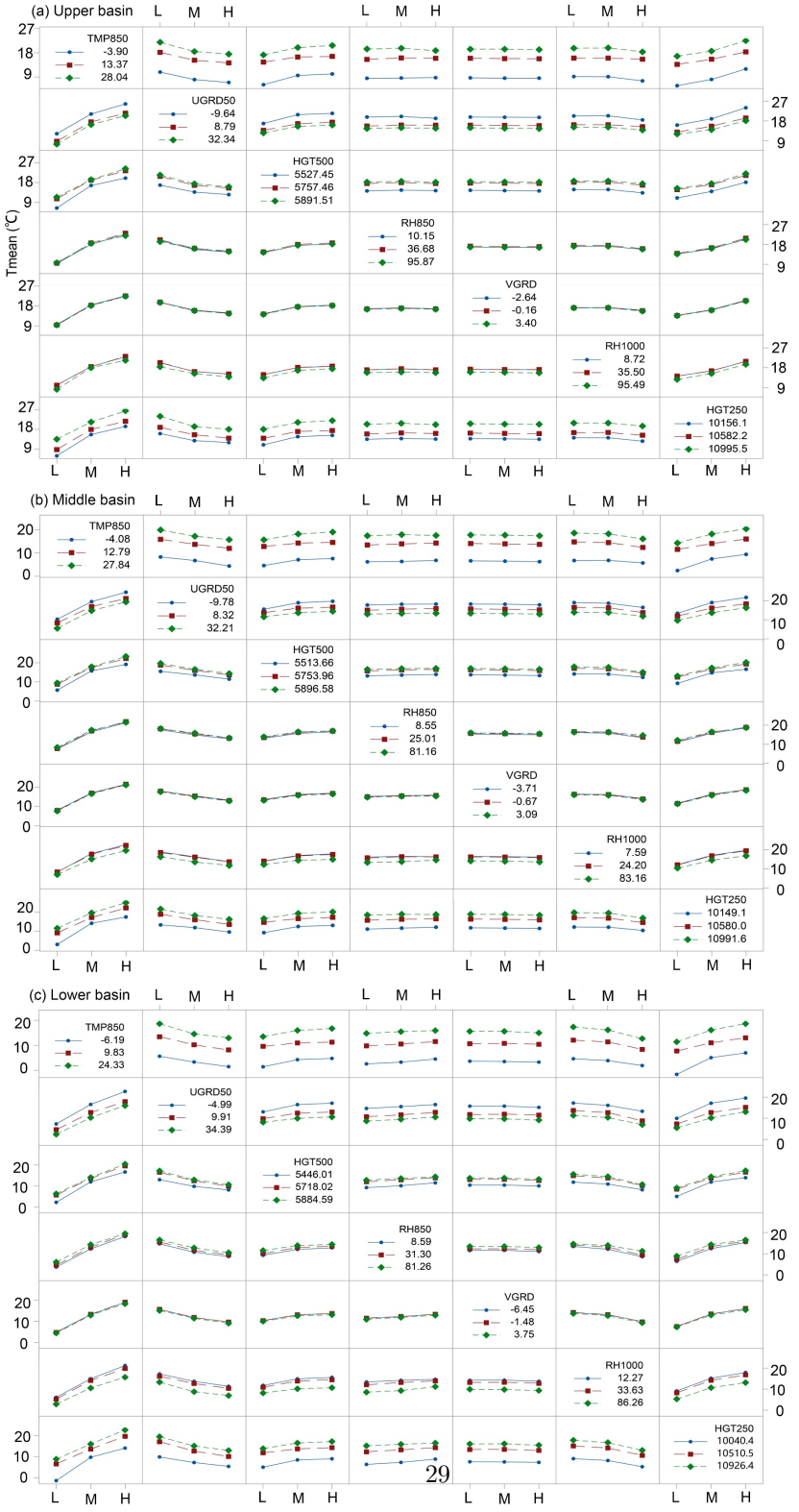
(a) Upper basin
TMP850
-3.90
13.37
28.04
UGRD50
-9.64
8.79
32.34
HGT500
5527.45
5757.46
5891.51
RH850
10.15
36.68
95.87
VGRD
-2.64
-0.16
3.40
RH1000
8.72
35.50
95.49
HGT250
10156.1
10582.2
10995.5
(b) Middle basin
TMP850
-4.08
12.79
27.84
UGRD50
-9.78
8.32
32.21
HGT500
5513.66
5753.96
5896.58
RH850
8.55
25.01
81.16
VGRD
-3.71
-0.67
3.09
RH1000
7.59
24.20
83.16
HGT250
10149.1
10580.0
10991.6
(c) Lower basin
TMP850
-6.19
9.83
24.33
UGRD50
-4.99
9.91
34.39
HGT500
5446.01
5718.02
5884.59
RH850
8.59
31.30
81.26
VGRD
-6.45
-1.48
3.75
RH1000
12.27
33.63
86.26
HGT250
10040.4
10510.5
10926.4
Tmean (°C)
L M H

Figure 13. The interactive effects of factors on the Tmean projectios.

Table 1. Potential factors selected for statistical downscaling models.

Factors selected	Unit	Pressure level (hPa)	Abbreviation
Relative humidity	%	1000	RH_1000
		850	RH_850
		500	
Air temperature	K	850	TMP_850
		700	
		500	
		250	
		10	
U-wind	m/s	100	
		50	UGRD_50
		10	
Geopotential height	m	850	
		700	
		500	HGT_500
		250	HGT_250
		100	
		50	
		10	
V-wind	m/s	10 m	VGRD

Table 2. The Calibration and validation statistics indicators for GCMs' reproductions for Tmean with NCEP reanalysis datasets.

Station	Calibration	Validation						
	R^2	NSE	STD	RMSE	R^2	NSE	STD	RMSE
P01	0.94	0.93	11.57	4.27	0.92	0.89	11.39	4.7
P02	0.95	0.94	11.70	3.85	0.92	0.91	11.24	4.62
P03	0.96	0.94	11.88	3.65	0.92	0.91	11.74	4.79
P04	0.95	0.94	10.60	3.48	0.92	0.88	10.51	4.43
P05	0.96	0.93	10.30	3.03	0.94	0.93	10.04	3.5
P06	0.95	0.92	9.96	3.15	0.92	0.88	9.81	4.01
P07	0.97	0.93	9.40	2.41	0.96	0.95	9.29	2.58
P08	0.96	0.92	9.81	6.06	0.95	0.91	9.55	6.33
P09	0.93	0.90	10.54	3.96	0.86	0.83	11.86	7.73
P10	0.88	0.92	9.71	3.05	0.94	0.90	9.72	3.56
P11	0.97	0.94	9.46	2.26	0.96	0.94	9.4	2.9
P12	0.96	0.92	8.91	2.46	0.93	0.90	8.9	3.09

Table 3. Projected trends in Tmean of decadal for the 12 stations under 4 scenarios (2021−2100).

GCMs	Scenarios	P01	P02	P03	P04	P05	P06	P07	P08	P09	P10	P
BCC-CSM	SSP1-2.6	0.009	0.008	0.009	0.008	0.007	0.007	0.008	0.008	0.007	0.007	0
	SSP2-4.5	0.026	0.026	0.031	0.026	0.026	0.026	0.026	0.027	0.028	0.027	0
	SSP3-7.0	0.043	0.043	0.049	0.043	0.041	0.040	0.040	0.040	0.041	0.038	0
	SSP5-8.5	0.054	0.054	0.061	0.054	0.051	0.049	0.048	0.049	0.047	0.049	0
CanESM5	SSP1-2.6	0.017	0.017	0.019	0.016	0.016	0.015	0.016	0.016	0.018	0.017	0
	SSP2-4.5	0.108	0.108	0.114	0.101	0.097	0.095	0.091	0.093	0.094	0.095	0
	SSP3-7.0	0.082	0.082	0.088	0.077	0.075	0.073	0.071	0.071	0.072	0.074	0
	SSP5-8.5	0.045	0.045	0.046	0.041	0.039	0.038	0.037	0.036	0.040	0.038	0
EC-Earth3	SSP1-2.6	0.022	0.021	0.023	0.020	0.018	0.018	0.018	0.017	0.017	0.018	0
	SSP2-4.5	0.037	0.037	0.041	0.036	0.035	0.033	0.031	0.033	0.032	0.032	0
	SSP3-7.0	0.054	0.053	0.061	0.054	0.051	0.050	0.049	0.053	0.050	0.052	0
	SSP5-8.5	0.073	0.071	0.082	0.072	0.069	0.067	0.066	0.069	0.067	0.066	0
INM-CM	SSP1-2.6	0.005	0.005	0.006	0.006	0.006	0.006	0.006	0.007	0.005	0.007	0
	SSP2-4.5	0.029	0.029	0.031	0.027	0.026	0.025	0.025	0.025	0.024	0.024	0
	SSP3-7.0	0.044	0.044	0.048	0.042	0.039	0.038	0.036	0.038	0.034	0.037	0
	SSP5-8.5	0.045	0.044	0.051	0.045	0.043	0.041	0.039	0.042	0.042	0.041	0
MPI-ESM	SSP1-2.6	0.008	0.009	0.008	0.008	0.007	0.006	0.007	0.007	0.008	0.006	0
	SSP2-4.5	0.022	0.022	0.024	0.023	0.022	0.021	0.019	0.019	0.021	0.022	0
	SSP3-7.0	0.043	0.042	0.048	0.043	0.044	0.043	0.040	0.040	0.041	0.045	0
	SSP5-8.5	0.054	0.054	0.062	0.055	0.053	0.050	0.049	0.049	0.052	0.052	0
ACCESS-CM2	SSP1-2.6	0.020	0.023	0.021	0.023	0.021	0.022	0.021	0.021	0.019	0.020	0
	SSP2-4.5	0.042	0.043	0.041	0.046	0.040	0.039	0.037	0.041	0.036	0.038	0
	SSP3-7.0	0.064	0.067	0.064	0.072	0.063	0.061	0.059	0.064	0.056	0.059	0
	SSP5-8.5	0.079	0.083	0.076	0.088	0.077	0.072	0.070	0.077	0.068	0.070	0
IPSL-CM6A	SSP1-2.6	0.015	0.013	0.016	0.013	0.012	0.010	0.010	0.009	0.008	0.011	0
	SSP2-4.5	0.035	0.033	0.036	0.034	0.031	0.029	0.029	0.029	0.027	0.030	0
	SSP3-7.0	0.067	0.065	0.071	0.064	0.060	0.058	0.056	0.058	0.057	0.058	0
	SSP5-8.5	0.086	0.085	0.098	0.086	0.081	0.078	0.078	0.079	0.079	0.079	0
MIROC6	SSP1-2.6	0.012	0.012	0.014	0.012	0.011	0.011	0.011	0.012	0.010	0.011	0
	SSP2-4.5	0.023	0.023	0.024	0.021	0.020	0.019	0.019	0.018	0.018	0.018	0
	SSP3-7.0	0.030	0.029	0.035	0.032	0.029	0.029	0.027	0.028	0.026	0.028	0
	SSP5-8.5	0.052	0.050	0.057	0.051	0.047	0.046	0.044	0.043	0.043	0.043	0
CAMS-CSM	SSP1-2.6	0.003	0.005	0.006	0.006	0.007	0.007	0.007	0.007	0.006	0.008	0
	SSP2-4.5	0.013	0.013	0.016	0.014	0.014	0.014	0.014	0.015	0.014	0.014	0
	SSP3-7.0	0.038	0.036	0.042	0.037	0.035	0.034	0.033	0.035	0.033	0.034	0
	SSP5-8.5	0.046	0.045	0.050	0.045	0.042	0.041	0.040	0.042	0.041	0.041	0
CESM2	SSP1-2.6	0.008	0.008	0.009	0.008	0.008	0.007	0.008	0.007	0.007	0.007	0
	SSP2-4.5	0.023	0.024	0.025	0.023	0.022	0.021	0.020	0.020	0.020	0.021	0
	SSP3-7.0	0.048	0.048	0.052	0.046	0.044	0.042	0.042	0.043	0.042	0.044	0
	SSP5-8.5	0.070	0.071	0.083	0.068	0.069	0.067	0.065	0.065	0.063	0.070	0
NorESM2	SSP1-2.6	0.005	0.005	0.005	0.003	0.004	0.004	0.003	0.004	0.003	0.003	0

GCMs	Scenarios	P01	P02	P03	P04	P05	P06	P07	P08	P09	P10	P
	SSP2-4.5	0.024	0.025	0.027	0.023	0.023	0.022	0.020	0.021	0.023	0.022	0
	SSP3-7.0	0.044	0.043	0.049	0.044	0.041	0.039	0.038	0.040	0.038	0.038	0
	SSP5-8.5	0.066	0.066	0.073	0.065	0.062	0.059	0.054	0.059	0.058	0.057	0
IITM-ESM	SSP1-2.6	0.036	0.037	0.040	0.036	0.035	0.034	0.033	0.035	0.037	0.037	0
	SSP2-4.5	0.019	0.018	0.023	0.019	0.021	0.020	0.019	0.020	0.021	0.022	0
	SSP3-7.0	0.036	0.037	0.039	0.034	0.034	0.033	0.032	0.033	0.034	0.036	0
	SSP5-8.5	0.045	0.046	0.050	0.044	0.043	0.042	0.041	0.042	0.041	0.046	0
Ensemble	SSP1-2.6	0.013	0.013	0.014	0.012	0.012	0.011	0.011	0.011	0.011	0.012	0
	SSP2-4.5	0.034	0.034	0.036	0.033	0.031	0.030	0.029	0.030	0.030	0.030	0
	SSP3-7.0	0.050	0.049	0.054	0.049	0.046	0.045	0.043	0.045	0.044	0.045	0
	SSP5-8.5	0.059	0.059	0.065	0.059	0.056	0.054	0.052	0.054	0.053	0.054	0

Journal of Geophysical Research - Atmospheres

Supporting Information for

Uncertainty Assessments of Multi-GCM, Multi-Scenario, and Multi-Factor for Temperature Projections: an Integrated SCA-WME-MFA Method

H. Wang1, Y. P. Li1,2, Y. R. Liu1, G. H. Huang1,2

1Environment and Energy Systems Engineering Research Center, School of Environment, Beijing Normal University, Beijing 100875, China

2Institute for Energy, Environment and Sustainable Communities, University of Regina, Regina, Saskatchewan S4S0A2, Canada

Contents of this file

Introduction

[Type or paste your text here. The introduction gives a brief overview of the supporting information. You should include information about as many of the following as possible (when appropriate):

- a general overview of the GCMs datasets;
- a general description of temperature projections;
- The results of Mann-Kendall test under different scenarios

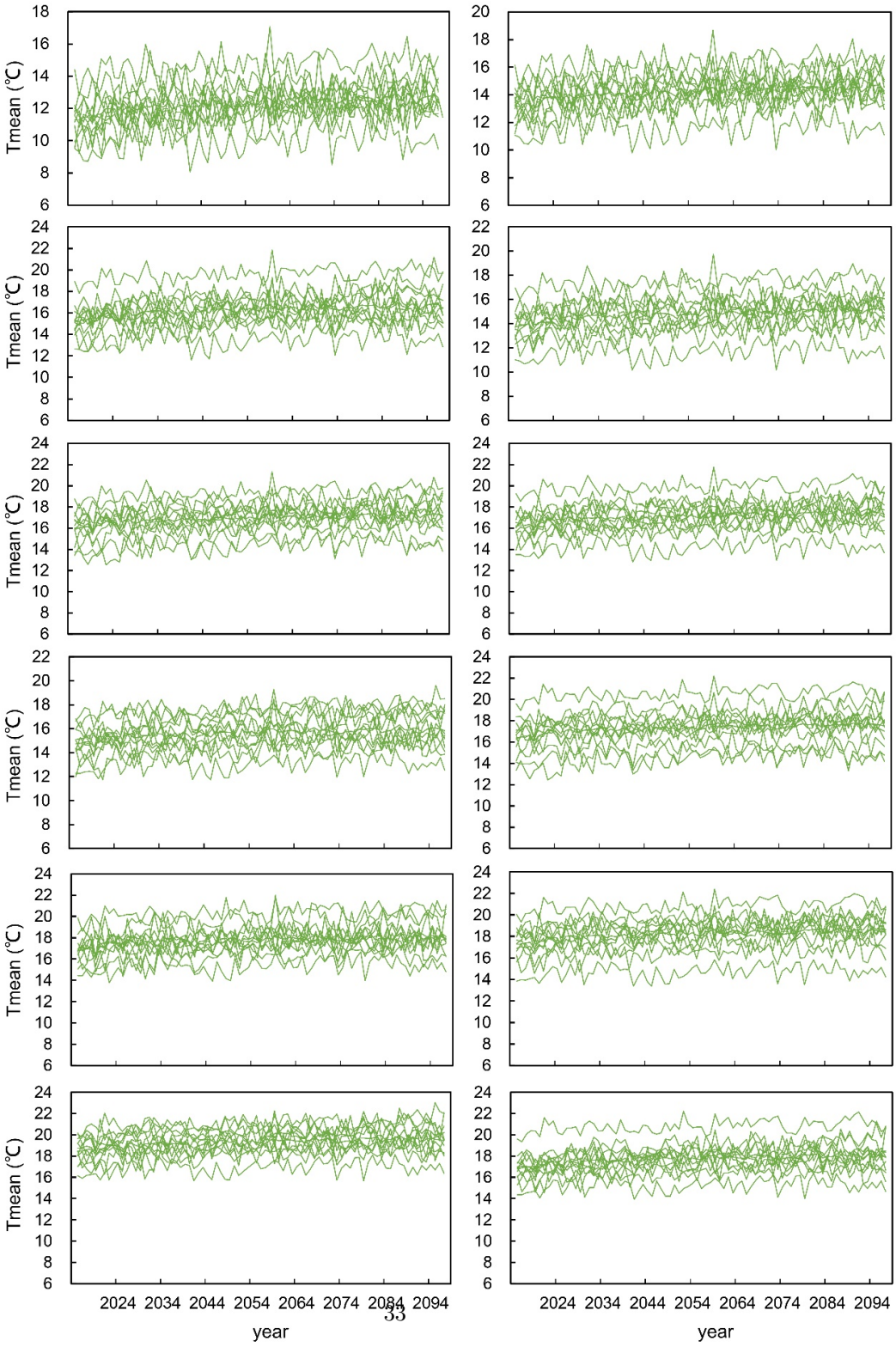
Tmean (℃)
year
2024 2034 2044 2054 2064 2074 2084 2094

Figure S1. Annual temperature projections of all GCMs under SSP1-2.6..

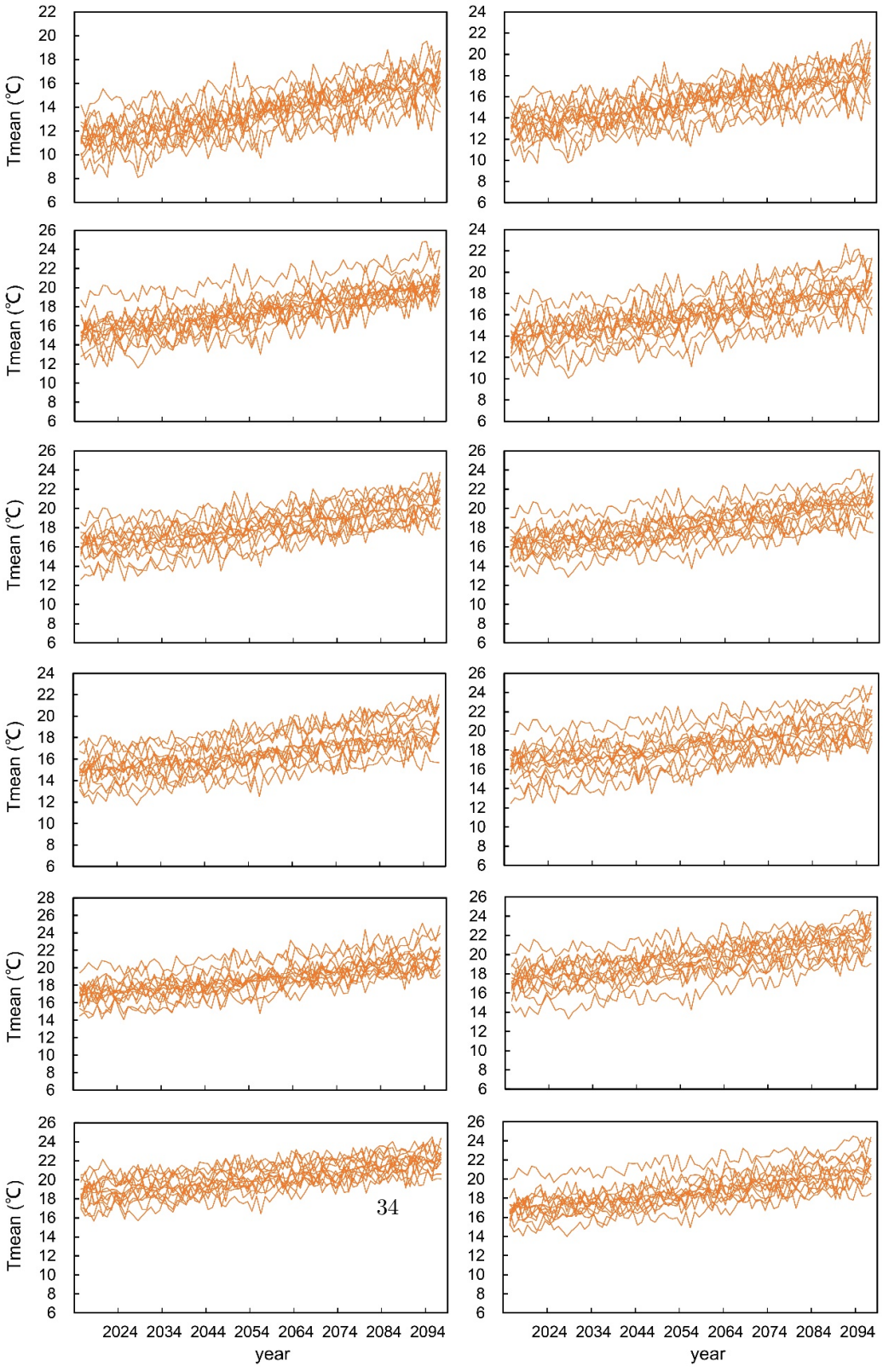

Figure S2. Annual temperature projections of all GCMs under SSP5-8.5.

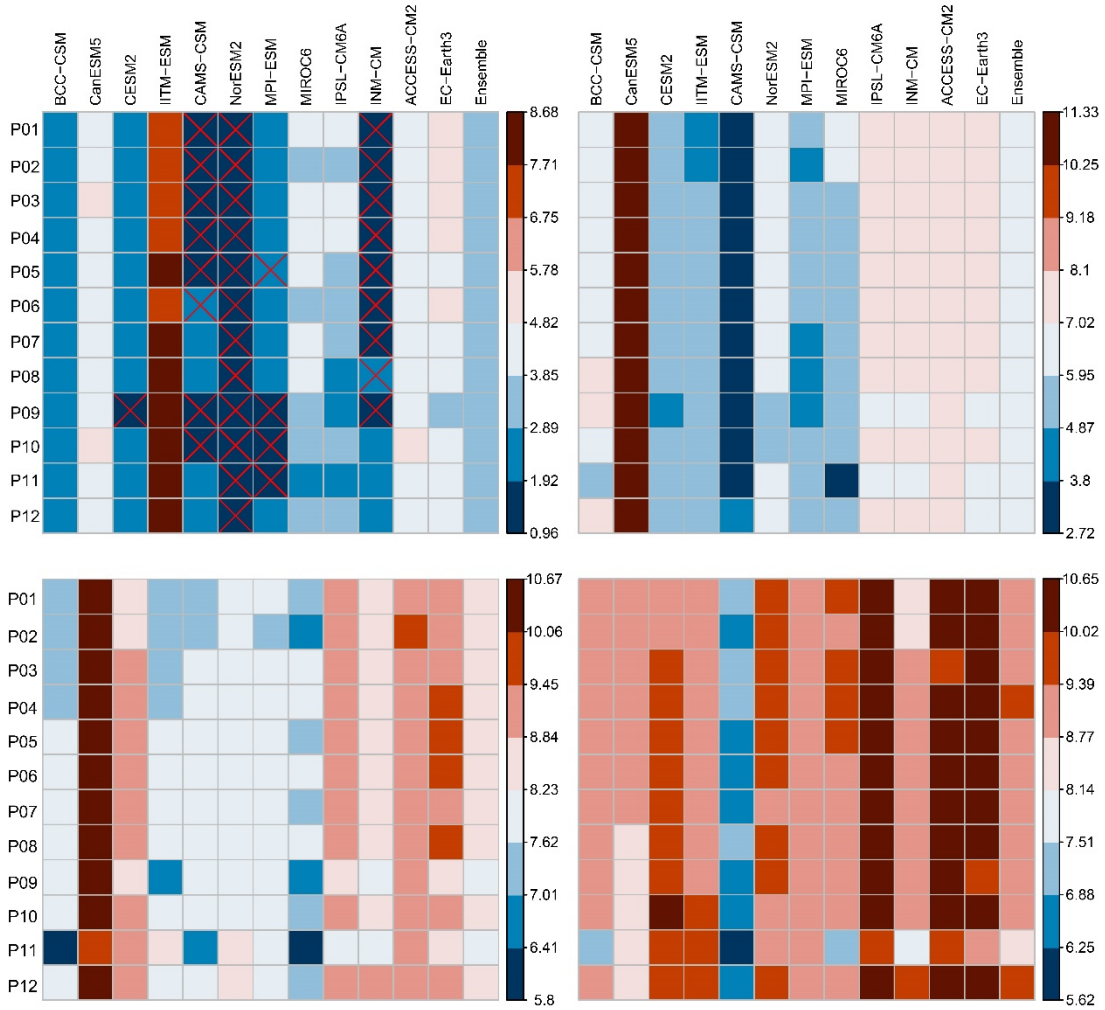

Figure S3. The results of Mann-Kendall test under different scenarios (The crosses indicate the MK p value > 0.05).

Table S1. The meteorological stations selected for study.

Number	ID	Name	latitude	longitude
25	P01	CIMBAJ, Uzbekistan	42.95	59.82
31	P02	TAHIATASH, Uzbekistan	42.40	59.60
32	P03	TAMDY, Uzbekistan	41.73	64.62
41	P04	DARGANATA, Uzbekistan	40.47	62.28
61	P05	KARAKUL, Uzbekistan	39.50	63.85
62	P06	CHARDZHEV, Tajikistan	39.08	63.60
64	P07	SAMARKAND, Uzbekistan	39.57	66.95
69	P08	CHIMKURGAN, Uzbekistan	38.80	66.20
70	P09	DECHANABAD, Uzbekistan	38.40	66.50
72	P10	KERKI, Tajikistan	37.83	65.20
74	P11	SHIRABAD, Uzbekistan	37.67	67.02
75	P12	SHURCHI, Uzbekistan	38.00	67.80

Table S2. The datasets of 12 global climate models used in this study.

Institution	Source (abbreviation in this paper)	Nominal resolution
Beijing Climate Center, China	BCC-CSM 2 MR (BCC-CSM)	km
Chinese Academy of Meteorological Sciences, China	CAMS-CSM 1.0 (CAMS-CSM)	km
Canadian Centre for Climate Modelling and Analysis, Environment and Climate Change, Canada	CanESM5	km
EC-Earth consortium, European Union	EC-Earth3-Veg (EC-Earth3)	km
Institute for Numerical Mathematics, Russian Academy of Science, Russia	INM-CM 4.8 (INM-CM)	km
Japan Agency for Marine-Earth Science and Technology, Japan	MIROC6	km
Max Planck Institute for Meteorology, Germany	MPI-ESM 1.2 (MPI-ESM)	km

Institution	Source (abbreviation in this paper)	Nominal resolution
National Center for Atmospheric Research, Climate and Global Dynamics Laboratory, USA	CESM2	km
Institute Pierre Simon Laplace, France	IPSL-CM6A-LR (IPSL-CM6A)	km
Commonwealth Scientific and Industrial Research Organization, Australia Australian Research Council Centre of Excellence for Climate System Science, Australia	ACCESS-CM2	km
Centre for Climate Change Research, Indian Institute of Tropical Meteorology Pune, India	IITM-ESM	km
NorESM Climate modeling Consortium	NorESM2-LM (NorESM2)	km